

The Mixing of Metastable States of Barium Atoms Induced by the ac Stark Effect

I. I. Bondar¹ and V. V. Suran¹

Physical Faculty, Uzhgorod State University, ul. Voloshina 54, Uzhgorod, 294000 Ukraine

Received November 15, 1999

Abstract—We present the results of experimental investigations of atoms perturbed by laser radiation under conditions when the energy of a Stark-shifted level becomes close to the energy of a neighboring level. © 2000 MAIK “Nauka/Interperiodica”.

PACS numbers: 32.60.+i, 32.80.–t

This paper presents the results of experimental studies of atoms perturbed by laser radiation under conditions when the change δE_n in the energy of some level n is comparable with the difference ΔE_{nk} between the energy of the considered level n and the neighboring level k (ΔE_{nk}), i.e., $\delta E_n \approx \Delta E_{nk}$. Note that this effect was theoretically predicted in [1, 2], but no experimental observation of this effect has been reported until recently.

We experimentally studied the perturbation of $6s5d^3D_1$ and $6s5d^3D_2$ metastable states of Ba atoms. To perturb these levels, we employed radiation of a color-center laser (CCL) with a frequency tunable within the range $\omega_1 = 8650 - 8900 \text{ cm}^{-1}$. The field strength of laser radiation in our experiments was equal to $\epsilon_1 = 5 \times 10^5 \text{ V/cm}$. The duration of laser pulses was $\tau = 4 \times 10^{-8} \text{ s}$. This radiation strongly perturbs the $6s5d^3D_2$ state of Ba atoms, since the frequency range covered by our laser includes the frequency $\omega_{nm} = 8845 \text{ cm}^{-1}$, which corresponds to a one-photon transition from the $6s5d^3D_2$ state to the $6s6p^1P_1^0$ state. Under these conditions, the dynamic polarizability α_n of the $6s5d^3D_2$ state should be large, and its frequency dependence can be represented as [2]

$$\alpha_n = \alpha_n(\omega) \approx \frac{(\omega_{nm} - \omega_1)d_{nm}^2}{(\omega_{nm} - \omega_1)^2 + \Gamma_m^2/4}, \quad (1)$$

where d_{nm} is the matrix element of the $6s5d^3D_2 \rightarrow 6s6p^1P_1^0$ transition and Γ_m is generally defined as the maximum among the width of the $6s6p^1P_1^0$ level and the line width of CCL radiation. As it follows from formula (1), the dynamic polarizability of the $6s5d^3D_2$ state is positive for frequencies $\omega_1 \leq \omega_{nm}$. Due to the ac

Stark effect, the change in the energy of this state ($\delta E = -\alpha_n \epsilon^2/4$, where ϵ is the strength of the CCL radiation field) should be negative in the considered spectral range. In particular, as the CCL field strength grows within a laser pulse, the energy of the $6s5d^3D_2$ state decreases, approaching the energy of the neighboring $6s5d^3D_1$ state.

Note that, within the range of frequencies $\omega_1 \leq \omega_{nm}$, the dynamic polarizability of the $6s5d^3D_1$ level (α_k) is described by a formula similar to (1). This polarizability is also positive due to the fact that the condition $\omega_1 \leq \omega_{km}$, where ω_{km} is the frequency of a one-photon transition from the $6s5d^3D_1$ state to the $6s6p^1P_1^0$ state ($\omega_{km} = 9027 \text{ cm}^{-1}$), is satisfied for frequencies from the above-specified range. In other words, similar to the energy of the $6s5d^3D_2$ level, the energy of the $6s5d^3D_1$ level also decreases under the action of CCL radiation.

However, according to our estimates, the dynamic polarizability of the $6s5d^3D_2$ state in the above-specified spectral range is much higher than the dynamic polarizability of the $6s5d^3D_1$ state. This difference between the polarizabilities of the considered states is due to two factors. First, within the studied frequency range, the detuning $\omega_1 - \omega_{km}$ for the $6s5d^3D_1$ level is greater than the detuning $\omega_1 - \omega_{nm}$ for the $6s5d^3D_2$ level. Second, as follows from [3], the matrix element d_{nm} for the $6s5d^3D_2 \rightarrow 6s6p^1P_1^0$ transition is 5.5 times higher than the matrix element d_{km} for the $6s5d^3D_1 \rightarrow 6s6p^1P_1^0$ transition. Our estimates show that the dynamic polarizability of the $6s5d^3D_1$ state in the above-specified spectral range is approximately 80 times lower than the dynamic polarizability of the $6s5d^3D_2$ state.

Note that the condition $\delta E_n \approx \Delta E_{nk}$ can be satisfied for perturbed $6s5d^3D_2$ levels under our experimental

¹ e-mail: qel@iss.univ.uzhgorod.ua

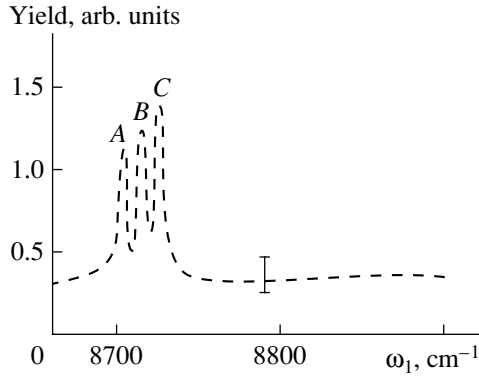


Fig. 1. The yield of Ba^+ ions produced under the joint action of CCL and DL beams on Ba atoms as a function of the frequency of CCL radiation.

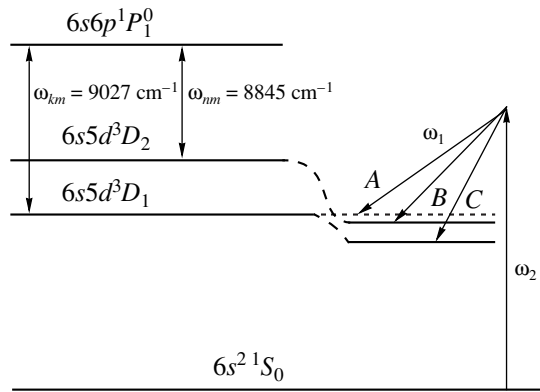


Fig. 2. Diagram of perturbation and excitation of Ba atoms. The left-hand part of the diagram corresponds to an unperturbed Ba atom, while the right-hand part corresponds to perturbed atoms. The dashed line shows the way the energies of $6s5d^3D_1$ and $6s5d^3D_2$ states change with the increase in ϵ .

conditions if the dynamic polarizability of the considered state is equal to $a \approx 5 \times 10^3$ au. Such a value of dynamic polarizability is quite realistic for triplet states of Ba atoms in the neighborhood of frequencies ω_{nm} corresponding to triplet–singlet transitions [4].

Thus, as the CCL field strength grows within a laser pulse under our experimental conditions, the shift of the $6s5d^3D_2$ level exceeds the shift of the $6s5d^3D_1$ level, and the energies of these two states may become approximately equal to each other with some CCL field strength.

The results of perturbation by a laser field were studied in our experiments by means of ionization resonance spectroscopy. We determined the frequencies of maxima in the yield of Ba^+ ions emerging from the ionization of perturbed states. Perturbed states of Ba atoms in these experiments were excited by the joint action of CCL radiation with the above-specified parameters and radiation of a dye laser (DL) with a fixed frequency

($\omega_2 = 17735 \text{ cm}^{-1}$). The field strength of DL radiation was equal to $\epsilon_2 = 4 \times 10^6 \text{ V/cm}$. The duration of DL pulses was equal to the duration of CCL pulses, $\tau = 4 \times 10^{-8} \text{ s}$. Our analysis shows that the perturbation of Ba atoms (including the perturbation of $6s5d^3D_1$ states) due to the action of DL radiation is much weaker than the perturbation of these atoms due to the action of CCL radiation.

The joint action of CCL and DL radiation on Ba atoms may give rise to a stimulated Raman scattering (SRS) process, when a Ba atom absorbs one photon of DL radiation and emits one photon at the frequency of CCL radiation. This process leads to the excitation of perturbed $6s5d^3D_1$ and $6s5d^3D_2$ states. These states were then ionized by CCL radiation and DL light. We brought light beams of these lasers into a spatial coincidence and focused them into the center of Ba atoms. Both laser beams were linearly polarized, and the vectors of the light fields in these beams were parallel to each other. Except for the parameters specified above, the arrangement of our experiments was identical to the experimental scheme described elsewhere [5].

The results of our measurements are shown in Fig. 1. As can be seen from these data, three resonance maxima are observed in the yield of Ba^+ ions. The frequencies of CCL radiation corresponding to these maxima are equal to 8705, 8715, and 8725 cm^{-1} . Note that none of these maxima coincides in frequency with maxima that could arise due to the excitation of Ba atoms by CCL radiation alone (see, e.g., the data presented in [6, 7]). Thus, all the three maxima in Fig. 1 are due to the excitation caused by the joint action of CCL and DL radiation on Ba atoms. Our analysis shows that only one of these maxima can be attributed to the excitation of an unperturbed state: the maximum at the frequency $\omega_1 = 8705 \text{ cm}^{-1}$ (maximum A in Fig. 1) is related to the excitation of the unperturbed $6s5d^3D_1$ state through the above-described SRS process (the relevant excitation scheme is shown in Fig. 2). The frequency of CCL radiation corresponding to this process is equal to $\omega_1 = 8702 \text{ cm}^{-1}$. The formation of Ba^+ ions contributing to this maximum occurs in the area where the field strength of CCL radiation interacting with a beam of Ba atoms is rather low.

We should note that, in accordance with selection rules for transitions in the presence of two radiation fields [8], the excitation of the $6s5d^3D_1$ state is forbidden in the case of parallel light field vectors. The appearance of a resonance maximum in this case can be explained by deviations from the parallel orientation of light field vectors and a large interaction volume, where the unperturbed $6s5d^3D_1$ state is populated in the presence of CCL radiation with a moderate field strength. Note that this effect was observed earlier in our study [5], where SRS was implemented for other states of Ba atoms.

Now, let us consider the resonance maxima B and C in Fig. 1. Our analysis shows that these maxima are related to the excitation of perturbed $6s5d^3D_1$ and $6s5d^3D_2$ states in a situation when the shift of the $6s5d^3D_2$ state meets the condition $\delta E_n \approx \Delta E_{nk}$. The corresponding excitation schemes are labeled as B and C in Fig. 2. The formation of Ba^+ ions in this case occurs in the interaction area where the field strength of CCL radiation interacting with a beam of Ba atoms is high. Note that the volume of this area is small as compared to the total volume of the area where CCL and DL beams are brought into a spatial coincidence.

In accordance with the theory presented in [1], the specific features of the perturbation of two levels n and k with a difference of total angular momenta ΔJ not exceeding 2 are determined in the case when $\delta E_n \approx \Delta E_{nk}$ by the interaction of these two states with the field of laser radiation. In particular, the shifts of each of these levels in such a situation depend on the dynamic polarizabilities of both levels (n and k) and the matrix element of the two-photon transition between these states, $V_{nk}^{(2)} = V_{nk}^{(2)}(\omega) + V_{kn}^{(2)}(-\omega)$. Therefore, even states with low dynamic polarizabilities may be subject to considerable shifts. In addition, the interaction of such states with the field of laser radiation cannot lead to the intersection of these states. The difference in the energies of such states under these conditions is determined by the relevant two-photon matrix element.

The experimentally observed dependences corresponding to the processes B and C are consistent with the above-described scenario of perturbation. Specifically, the frequencies of both maxima differ from the frequencies corresponding to the excitation of unperturbed $6s5d^3D_1$ and $6s5d^3D_2$ states. A small frequency difference characteristic of the considered maxima B and C ($\Delta\omega \approx 10 \text{ cm}^{-1}$) may be due to the smallness of the relevant two-photon matrix element $V_{nk}^{(2)}$.

The fulfillment of the condition $\delta E_n \approx \Delta E_{nk}$ also implies that the states n and k are mixed. The wave function of each of these states in such a situation can be represented as a superposition of the wave functions of both unperturbed states. The fact that the amplitudes

of the considered maxima are approximately equal to each other indicates that the effect described above plays a noticeable role in our experiments. If the levels under study were not mixed, the amplitudes of the relevant maxima would considerably differ from each other, since, in accordance with selection rules for parallel polarizations of light field vectors, excitation is allowed for the $6s5d^3D_2$ state and forbidden for the $6s5d^3D_1$ state [8]. Note that this alternative scenario of excitation was observed in our earlier studies [9], where the dynamic polarizabilities of the states being excited were equal to zero. The amplitude of the resonance maximum related to the excitation of the $6s5d^3D_2$ state in this case is two orders of magnitude higher than the amplitude of the maximum associated with the excitation of the $6s5d^3D_1$ state.

Thus, the structure of resonances B and C can be satisfactorily described in terms of the mixing of $6s5d^3D_1$ and $6s5d^3D_2$ states under conditions when $\delta E_n \approx \Delta E_{nk}$.

REFERENCES

1. N. B. Delone and V. P. Kraĭnov, *Atom in a Strong Light Field* (Énergoatomizdat, Moscow, 1984).
2. L. P. Rapoport, B. A. Zon, and N. L. Manakov, *Theory of Multiphoton Processes in Atoms* (Atomizdat, Moscow, 1978).
3. A. Bizzarri and M. C. E. Huber, *Phys. Rev. A* **42**, 5422 (1990).
4. I. I. Bondar and V. V. Suran, *Opt. Spektrosk.* **85**, 357 (1998) [*Opt. Spectrosc.* **85**, 327 (1998)].
5. I. I. Bondar and V. V. Suran, *Zh. Éksp. Teor. Fiz.* **107**, 1484 (1995) [*JETP* **80**, 829 (1995)].
6. I. I. Bondar and V. V. Suran, *Zh. Éksp. Teor. Fiz.* **113**, 499 (1998) [*JETP* **86**, 276 (1998)].
7. I. I. Bondar and V. V. Suran, *Opt. Spektrosk.* **85**, 357 (1998) [*Opt. Spectrosc.* **85**, 327 (1998)].
8. A. Yu. Elizarov and N. A. Cherepkov, *Zh. Éksp. Teor. Fiz.* **96**, 1227 (1989) [*Sov. Phys. JETP* **69**, 695 (1989)].
9. V. V. Suran, I. I. Bondar, and M. I. Dudich, *Zh. Éksp. Teor. Fiz.* **109**, 393 (1996) [*JETP* **82**, 208 (1996)].

Translated by A. Zheltikov

Intermittence Phenomena in the Burgers Equation Involving Thermal Noise

I. V. Kolokolov¹

*Budker Institute of Nuclear Physics, Siberian Division, Russian Academy of Sciences,
pr. akademika Lavrent'eva 11, Novosibirsk, 630090 Russia*

Received November 26, 1999

Abstract—Leading terms of the asymptotic behavior of the pair and higher order correlation functions for finite times and large distances have been calculated for the Burgers equation involving thermal noise. It is shown that an intermittence phenomenon occurs, whereby certain correlation functions are much greater than their reducible parts. © 2000 MAIK “Nauka/Interperiodica”.

PACS numbers: 47.27. Ak

Considerable deviation of the statistics of fluctuating fields from the Gaussian form is usually referred to as the intermittence. This property is typical of the hydrodynamic systems in the state of developed turbulence [1–3]. Under such strongly nonequilibrium conditions, the intermittence is manifested, in particular, as the dominance of the irreducible parts of the fourth-order correlation functions for certain quantities over the corresponding reducible parts. As a rule, the simultaneous correlation functions were considered in the papers cited above.

In thermodynamic equilibrium, the simultaneous correlation functions for the local fluctuating fields, as the functions of distances between points, are of the order of their reducible parts even in the critical region, provided that these reducible parts are nonzero. This is the foundation for the renormalization group method taking into account interaction between fluctuations through renormalization of the local fields and the effective Hamiltonian [4].

Recently, Lebedev [5] showed that the behavior can be substantially different for different-time correlation functions for the equilibrium fluctuating quantities. He demonstrated that different-time correlation functions for the density of vortex charges may be much larger than their Gaussian parts in the low-temperature phase of two-dimensional Berezinskii–Costerlitz–Towless systems. The following physical explanation for such behavior was proposed in [5]: different-time correlation functions of all orders in the vicinity of a given space point at low temperature are determined by a single rare fluctuation. This interpretation concludes that the intermittence phenomena must be manifested by features in the equilibrium dynamics of a wide class of systems.

In this study, we consider evolution of a one-dimensional velocity field $u(t, x)$ according to the following Burgers equation involving thermal noise:

$$u_t + uu_x - \nu u_{xx} = \xi(t, x). \quad (1)$$

Here, ν is the dissipation constant that is assumed to be small and $\xi(t, x)$ is the random noise described by the Gaussian statistics and by the pair correlation function

$$\langle \xi(t, x)\xi(t_1, x_1) \rangle = -\nu\beta^{-1}\delta''(x-x_1)\delta(t-t_1). \quad (2)$$

The parameter β plays the role of inverse temperature and the simultaneous steady-state velocity distribution function $\mathcal{P}[u]$ has the form

$$\mathcal{P}[u] = \mathcal{N} \exp\{-\beta\mathcal{F}[u]\}, \quad \mathcal{F}[u] = \int dx u^2(x), \quad (3)$$

where \mathcal{N} is the normalization constant. The equality

$$\langle u(t, x)u(t, x') \rangle = (2\beta)^{-1}\delta(x-x'), \quad (4)$$

which follows from expression (3), corresponds to the total absence of correlation between the velocity values in different points at the same time instant. We have calculated certain asymptotes of the different-time pair, triple, and quadruple correlation functions for the field $u(t, x)$. The obtained results indicate that the intermittence phenomena in fact occur in the equilibrium dynamics of a system described by equation (1).

A dynamic scaling exponent of $z = 3/2$ for problem (1)–(2) was found in [6] based on dimensional estimates and Galilean invariance. Considering the spectrum $\omega \propto k^{3/2}$, Lebedev and L'vov [7] demonstrated the absence of logarithmic divergences in each order of the perturbation theory with respect to translation. Therefore, the ratio $\beta x^3/T^2$ is a dimensionless argument of the function $F_2(T, x) = \langle u(T, x)u(0, 0) \rangle$. First, we determine an unknown leading term of the asymptotic behavior F_2 at $\beta x^3/T^2 \gg 1$ and $\nu \rightarrow 0$. It follows from the latter

¹ e-mail: kolokolov@inp.nsk.su

relationship that contribution of the diffusion mechanism to establishing correlation between points 0 and x during the time interval T is negligible. The fact that T is also small means that we can neglect the effect of noise on the dynamics in the time interval $(0, T)$. In this case, $u(0, y)$ is a functional $u(T, x)$ (or vice versa) and a Gaussian form of statistics of the velocity field at the time instant T makes it possible to represent the different-time pair correlation function in the form

$$F_2(T, x) = (2\beta)^{-1} \left\langle \frac{\delta u(0, 0)}{\delta u(T, x)} \right\rangle. \quad (5)$$

For $v \rightarrow 0$, the variational derivative $\Theta(t, y) = \delta u(t, u)/\delta u(T, x)$ satisfies the continuity equation

$$\Theta_t + u\Theta_y + u_y\Theta = 0 \quad (6)$$

and the condition $\Theta(T, y) = \delta(x - y)$. A solution to this Cauchy problem is found by the method of characteristic curves and the correlation function $F_2(T, x)$ is determined in the form [8]

$$\begin{aligned} F_2(T, x) &= (2\beta)^{-1} \langle \Theta(0, 0) \rangle \\ &= (2\beta)^{-1} \left\langle \delta(x - y(T)) \left(\frac{\partial y(T, \zeta)}{\partial \zeta} \right)_{\zeta=0} \right\rangle. \end{aligned} \quad (7)$$

Here, $y(T, \zeta)$ is the position of a Lagrangian particle leaving the point with the coordinate ζ at the moment $t = 0$

$$\dot{y} = u(t, y), \quad y(0, \zeta) = \zeta, \quad (8)$$

where $y(T) = y(T, 0)$. If $u(t, y)$ is discontinuous, equation (8) requires an extension of the definition. Bauer and Bernard [9] formally justified a physically obvious condition that the velocity of a Lagrangian particle at a discontinuity is equal to the velocity of motion of the discontinuity itself.

We conclude from expression (7) that the correlation function F_2 in the limit under consideration is determined by the most probable initial fluctuation of the velocity $u_0(y)$ that, evolving, transfers the particle from the point 0 to the point x in a time T . The probabilities of the initial distributions of the velocity field are specified by functional (3). We demonstrate that the desired optimum fluctuation $u_0(y)$, minimizing $\mathcal{F}[u_0]$ under the condition $y(T) = x$, has the form of a linear profile

$$\begin{aligned} u_0(y) &= u_0^* \equiv x/T - y/T, \quad 0 < y < x, \\ u_0(y) &= 0, \quad y < 0, y > x. \end{aligned} \quad (9)$$

Indeed, it is obvious that the function $u_0(y)$ must attain the maximum at $y = 0$. The zero value of the function $u_0(y)$ at $y < 0$ and $y > x$ is easily explained: nonzero values of the function $u_0(y)$ beyond the interval $(0, x)$ do not affect the trajectory $y(t)$, but increase the $\mathcal{F}[u_0]$ value. The left edge of the derived distribution $u(t, x)$ is a straight line characterized by the slope $\sigma = 1/t$ at any

time instant in the limit $v \rightarrow 0$. This time dependence is easily verified by direct substituting into the Burgers equation (see also [10]). The coordinate of the fastest point of the profile at $t = T$ is equal to x . The coordinates of all other points become the same. Therefore, for the initial data $u_0(y)$ belonging to the class described above, the plot of the function $u(T, y)$ has the form of the triangle

$$\begin{aligned} u(T, y) &= y/T, \quad 0 < y < x, \quad u_0(y) = 0, \\ & \quad y < 0, \quad y > x. \end{aligned} \quad (10)$$

Note now that the Burgers equation leads to the relation

$$d\mathcal{F}[u(t, y)]/dt = -2v \int dy u_y^2 \leq 0, \quad (11)$$

which yields

$$\mathcal{F}[u_0(y)] \geq \mathcal{F}[u(T, y)]. \quad (12)$$

This inequality is strict even in the limit $v \rightarrow 0$, provided that shock waves are formed during the evolution. Therefore, the minimum value of the functional \mathcal{F} is

$$\mathcal{F}[u(T, y)] = x^3/3T^2. \quad (13)$$

The functional \mathcal{F} value for the function $u_0^*(y)$ coincides with value (13) and the condition of forbidden formation of the shock waves during the time interval from 0 to T provides that expression (9) is the only possible form for $u_0(y)$.

The probability of initial fluctuation (9), being equal to $\exp(-\beta\mathcal{F}[u_0(y)])$, determines the exponential part of the asymptotic behavior of the pair correlation function F_2

$$F_2(T, x) \sim \exp\left(-\frac{\beta x^3}{3T^2}\right). \quad (14)$$

Note that the factor $(\partial y(T, \zeta)/\partial \zeta)_{\zeta=0}$ entering into formula (7) at the δ function vanishes for configuration (9), but it is nonzero at a small variation of $u_0(y)$. In other words, this factor, as well as the unknown pre-exponential factor in expression (14) as a whole, is determined by integration over the deviations δu of the initial velocity field with respect to $u_0^*(y)$. The typical δu values are small as compared to $u_0^*(y)$ with respect to the parameter $\beta x^3/T^2$. Nevertheless, the integration over δu is not reduced to the Gaussian form even in the limit $\beta x^3/T^2 \gg 1$. The reason is that the functional $\mathcal{F}[u]$ is nonanalytic in the limit $v \rightarrow 0$ for the class of functions $u(y)$ such that $y(T) = x$. The variation $\delta\mathcal{F}$ is of the first-order smallness in δu although the inequality $\delta\mathcal{F} \geq 0$ is still fulfilled. The functional $\mathcal{F}[u]$ can be expanded in the functional Taylor series in terms of δu only for $\delta u \ll v/x$. Corresponding analysis will be performed elsewhere and we restrict this consideration to exponential accuracy.

Noting that linear profile (9) transfers all points belonging to the interval $(0, x)$ to the point x by the time instant $t = T$, we obtain to within the exponential accuracy that

$$F_{n+2} = \left\langle u(T, x) \prod_{j=1}^n u(0, y_j) u(0, 0) \right\rangle \quad (15)$$

$$\sim F_2(T, x) \sim \exp\left(-\frac{\beta x^3}{3T^2}\right),$$

where $0 < y_1 < y_2 \dots < y_n$. The reducible part of this correlation function at $n \geq 1$ is obviously equal to zero. The same fluctuation $u_0^*(y)$ determines the following leading asymptotic behavior of the correlation function $\Phi_4 = \langle u(T, x)u(T, x+a_1)u(0, a)u(0, 0) \rangle$ for $0 < a < x$ and $0 < a_1 \ll a$

$$\Phi_4 \sim \exp\left(-\frac{\beta x^3}{3T^2}\right) \gg \Phi_{4, \text{Gauss}} \sim \exp\left(-\frac{2\beta x^3}{3T^2}\right). \quad (16)$$

Here, $\Phi_{4, \text{Gauss}}$ is the reducible part of the correlation function Φ_4 . To find the correlation function Φ_4 as a function of the parameter a , it is necessary to consider evolution of the perturbed linear profile; during this evolution, the reversal inevitably occurs and the problem becomes substantially more complex. We note also that dependence of the correlation function Φ_4 on a is related directly to the distribution function of the velocity field gradients; the latter function is determined, as was shown in [11, 12], by the shock waves being formed. Coincidence of the leading asymptotic terms of the pair and higher order correlation functions is typical of the turbulence problems, as was originally indicated for these problems in [13].

The correlation functions for the field $u(t, x)$ can be represented in the form of functional integrals (see, for example, [14]). These integrals are calculated, in essence, by the saddle point method, where the saddle-point parameter $\beta x^3/T^2 \gg 1$ is determined by the averaged quantity rather than by the action. This approach was originally proposed by Lifshits [15]. More recently, it was generalized to determine higher order correlation functions for both equilibrium [16] and substantially nonequilibrium systems [12, 17–22]. The optimal fluctuation is also referred to as instanton, the term generally accepted in the quantum field theory. The long-term asymptotic behavior of the autocorrelation function of the current through the disordered contact was calculated in [23], where large observation time interval was used as a saddle-point parameter determining the instanton.

This study was stimulated by numerous discussions with M. Chertkov and V. Lebedev. I am grateful to them for advice and critical comments. I am pleased to thank G. Falkovich and T. Spencer for inspiring support and to M. Stepanov for valuable remarks and suggestions.

REFERENCES

1. U. Frisch, *Turbulence. The Legacy of A. N. Kolmogorov* (Cambridge University, Cambridge, 1995).
2. M. Chertkov, G. Falkovich, I. Kolokolov, and V. Lebedev, Phys. Rev. E **52**, 4924 (1995).
3. K. Gawedzki and A. Kupiainen, Phys. Rev. Lett. **75**, 3834 (1995).
4. A. Z. Patashinskiĭ and V. L. Pokrovskiĭ, *Fluctuation Theory of Phase Transitions* (Nauka, Moscow, 1982).
5. V. V. Lebedev, cond-mat/9904430.
6. D. Forster, D. R. Nelson, and M. J. Stephen, Phys. Rev. A **16**, 732 (1977).
7. V. V. Lebedev and V. S. L'vov, Pis'ma Zh. Éksp. Teor. Fiz. **58**, 301 (1993) [JETP Lett. **58**, 310 (1993)].
8. Ya. B. Zel'dovich and A. D. Myshkis, *Elements of Mathematical Physics* (Nauka, Moscow, 1973).
9. M. Bauer and D. Bernard, chao-dyn/9812018 v2.
10. S. N. Gurbatov, A. N. Malakhov, and A. I. Saichev, *Nonlinear Random Waves in Nondispersion Media* (Nauka, Moscow, 1990).
11. E. Weinan, K. Khanin, A. Mazel, and Y. Sinai, Phys. Rev. Lett. **78**, 1904 (1997).
12. E. Balkovsky, G. Falkovich, I. Kolokolov, and V. Lebedev, Phys. Rev. Lett. **78**, 1452 (1997).
13. V. L'vov and G. Falkovich, Phys. Rev. A **46**, 4762 (1992).
14. E. I. Kats and V. V. Lebedev, *Dynamics of Liquid Crystals* (Nauka, Moscow, 1988).
15. I. M. Lifshits, Usp. Fiz. Nauk **83**, 617 (1964) [Sov. Phys. Usp. **7**, 571 (1965)].
16. L. N. Lipatov, Zh. Éksp. Teor. Fiz. **72**, 411 (1977) [Sov. Phys. JETP **45**, 216 (1977)].
17. V. Falko and K. Efetov, Europhys. Lett. **32**, 627 (1995).
18. G. Falkovich, I. Kolokolov, V. Lebedev, and A. Migdal, Phys. Rev. E **54**, 4896 (1996).
19. V. Gurarie and A. Migdal, Phys. Rev. E **54**, 4908 (1996).
20. M. Chertkov, Phys. Rev. E **55**, 2722 (1997).
21. E. Balkovsky and G. Falkovich, Phys. Rev. E **57**, 1231 (1998).
22. E. Balkovsky and V. Lebedev, Phys. Rev. E **58**, 5776 (1998).
23. B. A. Muzykantskiĭ and D. E. Khmel'nitskiĭ, Phys. Rev. B **51**, 5480 (1995).

Translated by R. Tyapaev

CONDENSED
MATTER

Energy, Compressibility, and Covalence in the Carbon Family

S. M. Stishov

*Institute for High-Pressure Physics, Russian Academy of Sciences, Troitsk, Moscow oblast, 142092 Russia
Los Alamos National Laboratory, P.O. Box 1663, Los Alamos, NM 87545, USA*

Received July 5, 1999; in final form, December 6, 1999

Abstract—It is shown that a similarity relationship of the type $(K_0V_0/E_0) \cong \text{const}$ (where K_0 , V_0 , and E_0 are the bulk modulus, the volume, and the total energy at $P = 0$) exists for the elements of the carbon family, including C, Si, Ge, Sn, and Pb. This fact rules out the possibility of significant covalent effects on the compressibility of the corresponding substances. The record bulk modulus value of diamond is associated with its extreme atomic density. © 2000 MAIK “Nauka/Interperiodica”.

PACS numbers: 62.20.Dc

It is commonly argued that covalent interaction is responsible for the formation of a substance that possess a high modulus of elasticity. Diamond is frequently used in this case as a typical example. It is a “perfect” covalent crystal and can be characterized as the least compressible substance in the available part of the Universe. Below, I will show using the carbon family elements as an example that this statement is not true in the general case. It turns out that the bulk modulus in the C–Si–Ge–Sn–Pb series of the carbon family elements is directly proportional to the energy density with a virtually universal factor of proportionality. Generally speaking, this fact is not favorable to the idea of a significant contribution of covalent effects to the compressibility of the corresponding substances.

Let us obtain a relationship between the bulk modulus K and the total energy E_t in the case of a general $E_t(V)$ dependence. The total energy of a substance at $T = 0$ may be written as

$$E_t = E_0 f(V/V_0), \quad (1)$$

where E_0 and V_0 are the total energy and the volume of the substance at $P = 0$ and $T = 0$. Hence, the bulk modulus can be written as follows:

$$K = V(\partial^2 E_t / \partial V^2)_T = (E_0/V_0)(V/V_0) f''(V/V_0). \quad (2)$$

At $P = 0$, this expression is reduced to

$$K_0 = (E_0/V_0) f''_0(V/V_0)_{V=V_0} \quad (3)$$

or

$$(K_0V_0/E_0) = f''(V/V_0)_{V=V_0}. \quad (4)$$

From (1) and (4), it follows that, if the function $f(V/V_0)$ is universal for a certain set of substances, then the ratio K_0V_0/E_0 transforms to the similitude relationship $(K_0V_0/E_0) = \text{const}$. It is easy to calculate the corresponding values with the help of tabulated data, which is what I will do below. However, I will first indicate that, in line with the physical description of the structure of metals and semiconductors (a system of ions embedded in the liquid of valence electrons), the total energy in

this case is assumed to be equal to the difference between the ground-state energy and the energy of the system of noninteracting fourfold ionized ions and the corresponding number of electrons. According to the aforesaid, the total energy E_0 at $P = 0$ may be calculated as $E_0 = E_c + E_i$, where E_c is the cohesive energy and E_i is the fourfold ionization energy.

Figure 1 demonstrates the behavior of the value of K_0V_0/E_0 as a function of the atomic number of the carbon family elements. The table presents the corresponding numerical data. It is seen in the figure that the value of K_0V_0/E_0 varies only slightly as the atomic number of the element changes.¹ It is surprising that no discontinuity is observed in passing from covalent crystals (C, Si, Ge, and α -Sn) to good metals (β -Sn and Pb). Moreover, both white and gray tin, which represent “covalent” and metallic modifications of the same substance, are characterized by the same value of the K_0V_0/E_0 ratio. With regard to relationship (4), this means that the form of the function $E_t(V)$ describing the total energy of the carbon family elements does not change significantly within the group and that the similitude relationship of the form $(K_0V_0/E_0) \cong \text{const}$ holds true for the entire group as a whole. This conclusion is also based on the fact that the potential energy curves of all substances have, in some sense, a universal form that provides their stability. In this case, the equality of the second derivatives allows the conclusion, at least as a rather probable suggestion, that the function $E_t(V)$ is a universal function.²

¹ Note that the quantity $f''_0 = K_0V_0/E_0$ is rather sensitive to the form of the function $E_t(V)$. For example, it is easy to show that, for the function $E_t(V)$ of the form $E_t = (E_0/n - m)[m(V_0/V)^n - n(V_0/V)^m]$, the ratio $(K_0V_0/E_0) = mn$. In particular, for noble gases, it must be expected that $(K_0V_0/E_0) \approx 8$, which is observed in reality.

² In the case when the energy can be written as a combination of power functions, the second derivative of the energy with respect to the reduced volume at $V/V_0 = 1$ is expressible through the corresponding exponents (see footnote 1) and, hence, characterizes the entire potential curve as a whole.

Atomic volumes (V_0), bulk moduli (K_0), and total energies (E_0) for the carbon family elements at atmospheric pressure (values of V_0 and K_0 correspond to room temperature)

Substance	Atomic number	V_0 [1], cm ³ /g-atom	K_0 , Mbar	E_0 , eV*	K_0V_0/E_0
C (diamond)	6	3.42	4.43 [2]	155.4	0.101
Si	14	12.06	0.977 [3]	107.8	0.112
Ge	32	13.63	0.749 [3]	107.6	0.094
β -Sn	50	16.30	0.55 [3]	102.2	0.091
α -Sn	50	21.31	0.42 [4]	102.2	0.087
Pb	82	18.26	0.45 [1]	98.7	0.086

* The total energy E_0 was calculated as the sum $E_0 = E_c + E_I$, where E_c is the cohesive energy [3, 6], and E_I is the fourfold ionization energy [5].

Finally, the material presented here leads to the conclusion that specific covalent effects are not manifested in uniform deformation. The table and Fig. 1 demon-

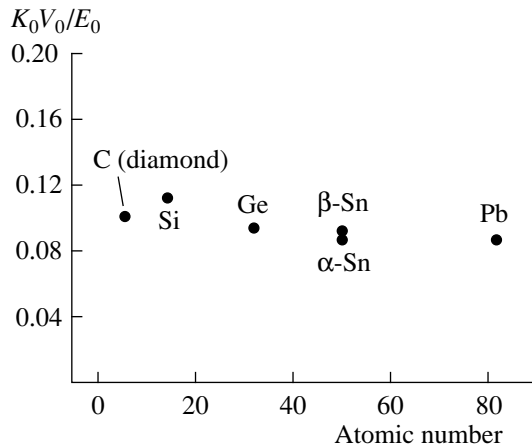


Fig. 1. Dependence of the K_0V_0/E_0 ratio on the atomic number of the carbon family elements.

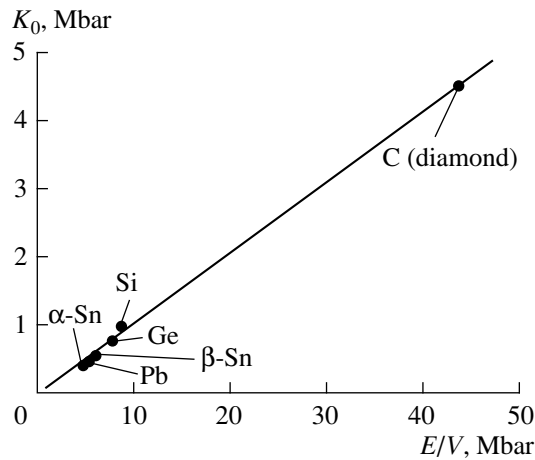


Fig. 2. Bulk modulus K_0 as a function of the energy density E_0/V_0 for the carbon family elements.

strate that the bulk modulus K_0 of the carbon family elements may be written as

$$K_0 \cong c(E/V)_0, \quad (5)$$

where $c \approx 0.1$, and $(E/V)_0$ is the energy density at $P = 0$. Relationship (5) is illustrated in Fig. 2. I emphasize that the exceptionally high value of the energy density in diamond is achieved to a great extent because of the extremely small value of the atomic volume of carbon (see table). Consequently, the record bulk modulus value of diamond is due to its extreme atomic density, which, in its turn, is associated with the electronic configuration of the carbon atom and is completely unrelated to covalent effects (also see discussion in [7]).

Note in conclusion that, in the light of the above, the possibility of creating carbon materials with a bulk modulus and a hardness exceeding the diamond values seems unlikely.

The author is grateful to V.V. Brazhkin and A.G. Lyapin for their help in work and numerous discussions.

REFERENCES

1. *Properties of Elements: Reference Book*, Ed. by M. E. Drifts (Metallurgiya, Moscow, 1997), Vol. 1.
2. H. J. McSkimin and P. Andreatch, Jr., *J. Appl. Phys.* **43**, 2944 (1972).
3. D. A. Young, *Phase Diagrams of the Elements* (Univ. of California Press, Berkeley, 1991).
4. R. Ravelo and M. Baskes, *Phys. Rev. Lett.* **79**, 2482 (1997).
5. *Tables of Physical Data: Reference Book*, Ed. by I. K. Kikoin (Atomizdat, Moscow, 1976).
6. W. A. Harrison, *Electronic Structure and the Properties of Solids: The Physics of the Chemical Bond* (Freeman, San Francisco, 1980).
7. M. T. Yin and M. L. Cohen, *Phys. Rev. Lett.* **50**, 2006 (1983).

Translated by A. Bagatur'yants

CONDENSED
MATTER

Effects of the Overlap between Wave Functions of Impurity Centers on the Activation Energy of Hopping Conduction

A. P. Mel'nikov*,¹ Yu. A. Gurvich*, L. N. Shestakov**, and E. M. Gershenzon*

* Moscow State Pedagogical University, Moscow, 119891 Russia

** Seaside State University, Arkhangel'sk, 163006 Russia

Received November 25, 1999

Abstract—The hopping conductivity σ_3 has been studied in samples of slightly counterdoped crystalline Si : B with a boron concentration of $2 \times 10^{16} \text{ cm}^{-3} < N < 10^{17} \text{ cm}^{-3}$ and a compensation of $10^{-4} \leq K \leq 10^{-2}$. It is found that at $K \leq 10^{-3}$ the activation energy ε_3 is not lower (as it must be according to classical notions at finite K) but larger than the value $\varepsilon_N = e^2 N^{1/3} / \kappa$, where e is the electronic charge and κ is the dielectric constant. With decreasing N , the energy ε_3 drops slower and, with decreasing K , grows faster than follows from the standard theory. At $K \leq 10^{-4}$, ε_3 is higher than ε_N by a factor of 1.5–2. The result is explained by the effect of the overlap between wave functions of neighboring impurity centers on the structure of the impurity band. © 2000 MAIK “Nauka/Interperiodica”.

PACS numbers: 72.20.E, 72.80.Jc

1. Impurity conduction in slightly doped crystalline semiconductors (σ) at low temperatures (T) occurs by electron hopping over the ground states of impurity centers. At a low compensation $K = N/N_K \ll 1$ (N and N_K are the concentrations of the majority and compensating impurities), it is convenient to speak about vacancy hopping. (We will put forth the presentation with reference to an n -type material.) The $\sigma(T)$ dependence corresponds to an activation process. The activation energy is conventionally designated as ε_3 . If the ground-state energy of an isolated donor is taken as zero, then the energy ε_3 at $T \rightarrow 0$ coincides with the Fermi energy μ . In the case of shallow donors at $K \rightarrow 0$,

$$\mu = \varepsilon_3 \approx \varepsilon_N \equiv e^2 N^{1/3} / \kappa, \quad (1)$$

where e is the electronic charge and κ is the dielectric constant of the crystal. With increasing K , the value of ε_3 slightly decreases: $\varepsilon_3 = \varepsilon_N(1 - 0.29K^{1/4})$ [1]. The results of measurements on samples with $0.01 \leq K \ll 1$ agree with the pattern described in [1]. Note that K is a small parameter in the standard theory of hopping conduction. With decreasing K , agreement between the theory and experiment must improve.

When studying the hopping conductivity in a great number of Si : B samples with $2 \times 10^{16} \text{ cm}^{-3} < N < 10^{17} \text{ cm}^{-3}$, we found that a discrepancy between the experiment and the theory arises at $K \leq 10^{-2}$, which become greater with decreasing K . Below, we will restrict our consideration to the description of results

obtained in low electric fields, where $\sigma_3(E) = \text{const}$. Figure 1 displays the dependence $\varepsilon_3(K)$ at $N = \text{const} = 3.6 \times 10^{16} \text{ cm}^{-3}$ (a set of samples with transmutation doping). In the same figure, the dashed line represents the dependence $\varepsilon_3(K)$ according to [1]. It is seen that agreement with the calculation is observed only at $K > 10^{-2}$. Note that, according to the theory, the ratio $\varepsilon_3/\varepsilon_N < 1$ and $\rightarrow 1$ at $K \rightarrow 0$ (see above). The experimental results indicate that, in samples with $K < 3 \times 10^{-3}$ $\varepsilon_3/\varepsilon_N < 1$ and the dependence on K is completely different. Figure 2 shows the dependence $\varepsilon_3(N)$ for samples with close values of K ($K \approx 10^{-3}$). The dashed line shows dependence (1). The calculated values for our K differ from (1) by no more than 5%. Note that the dependence $\varepsilon_3(N)$ at $K \approx \text{const}$ turns out to be weaker than (1).

2. Let us discuss the results obtained for samples with $K > 5 \times 10^{-4}$. In the theory of ε_3 -conduction, it is suggested that the structure of the impurity band is of purely classical origin and is determined exclusively by fluctuations of the Coulomb potential. At $K \ll 1$ and low T , all the acceptors are negatively charged. A vacancy is located in the vicinity of almost each acceptor. This is a neutral 1-complex (concentration $N_1 \sim N_K$). In the vicinity of some acceptors, vacancies are absent. These are negative 0-complexes (concentration N_0). There are acceptors binding two vacancies. These are positive 2-complexes (concentration N_2). The value $\mu = \varepsilon_3$ is determined from the neutrality equation

$$N_0(\mu) = N_2(\mu). \quad (2)$$

¹ e-mail: melnikov@rpl.mpgu.msk.su

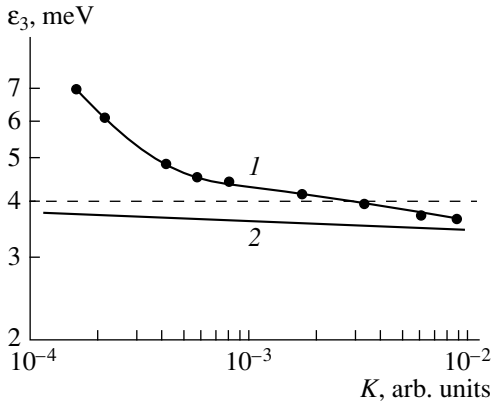


Fig. 1. (1) Dependence $\epsilon_3(K)$ for Si:B samples with $N = 3.6 \times 10^{16} \text{ cm}^{-3}$. (2) Calculated dependence $\epsilon_3(K)$. Dashed line shows the value $\epsilon_3 = \epsilon_N$.

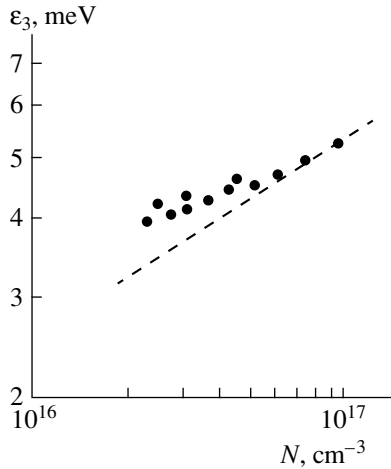


Fig. 2. Dependence $\epsilon_3(N)$ for Si:B samples with $K \approx 10^{-3}$. Dashed line shows the calculated dependence $\epsilon_3(N)$ at $K \rightarrow 0$.

The ratio $r_\mu/\bar{r} \equiv z$ is the characteristic parameter of the problem. Here, $r_\mu = e^2/\kappa\mu$ is the distance at which the additional Coulomb contribution to the energy of a neutral donor in the field of the acceptor equals μ , and $\bar{r} = (4\pi N/3)^{-1/3}$ is the average distance between donors. The equation for $N_0(\mu)$ takes the form

$$N_0 = N_K \exp(-v), \quad (3)$$

where $v = z^3$ is the average number of donors in the sphere of radius r_μ . Equations for $N_2(\mu)$ are given in [1]. Equality (1) is the solution of equation (2). It turns out that $N_0 = N_2 \approx 0.02N_K$.

This theory completely neglects the quantum effects, that is, the overlap between the wave functions of neutral centers. However, Coulomb fluctuations decrease at $K \rightarrow 0$, and the overlap effects become significant. Complexes of several neighboring neutral

centers arise in this case. The first ionization energy of such complexes may differ from the first ionization energy of an isolated donor. This will result in a change in the shape of the density of the impurity band $g(\epsilon)$ and in the appearance of states of charged formations of a different kind. As N_K decreases or N increases, it becomes necessary to give primary consideration to the most probable complexes of two neutral donors (D_2 -complexes).

The first ionization energy of a D_2 -complex depends on the distance ρ between donors. The difference of the first ionization energies of an isolated donor and a D_2 -complex $\Delta(\rho)$ has a maximum at $\rho = \rho_m \approx 4a_0$, equal to $\Delta(\rho_m) \equiv \Delta_m \approx 0.065\epsilon_1$, which makes up ≈ 3 meV for Si : B. Here, a_0 is the effective Bohr radius, and $\epsilon_1 = e^2/2\kappa a_0$ is the effective Rydberg constant. The dependence $\Delta(\rho)$ is shown in Fig. 3 [2, 3]. Below, D_2 -complexes for which $\Delta(\rho)$ is comparable with Δ_m will be named molecules. We denote their concentration by M .

Now, we are to discuss the effect of molecules on the density of states of the impurity band $g(\epsilon)$. Let us mentally switch off the overlap. In this case, we will have a set of noninteracting neutral centers, to which the standard theory of ϵ_3 -conduction can be applied. In this case, the density of states of the impurity band has a sharp peak at $\epsilon = 0$. Now, we switch on the overlap again. Molecules whose first ionization energies are lower than that of a neutral center will appear. This decrease means that part of states (of order M per unit volume) pass from the major peak to the region $\epsilon \leq \Delta_m$. An additional peak in $g(\epsilon)$ will form in this region [3].

It is convenient to consider the effect of molecules on μ separately for the cases $\epsilon_N < \Delta_m$ and $\epsilon_N > \Delta_m$. In the first case, as the overlap is switched on, part of states pass from the region $\epsilon < \mu = \epsilon_N$ to the region $\epsilon \approx \Delta_m > \mu$. It is evident that this must lead to an increase in μ at constant N and N_K . At large M/N_K , the level $\mu \rightarrow \Delta_m$. We will not consider this case in detail, because the inequality $\epsilon_N < \Delta_m$ is obeyed for Si : B ($a_0 = 23 \times 10^{-8} \text{ cm}$) at $N < 2 \times 10^{15} \text{ cm}^{-3}$. When N is so small, the hopping conductivity in Si:B cannot be measured.

Consider the case of $\epsilon_N > \Delta_m$. Under this condition, almost all molecules are neutral. An exception is provided by molecules whose distance from an acceptor is less than $r_{\mu-\Delta} = e^2/\kappa(\mu - \Delta(\rho))$. Almost all such molecules will be ionized. An acceptor can bind two vacancies, vacancy and an ionized molecule, or two ionized molecules. Thus, as the overlap is switched on, the concentration of positively charged complexes increases. At the same time, the overlap decreases the concentration of negatively charged complexes N_0 . In fact, the exponent in equation (3) is the probability that the sphere of radius r_μ contains no donor. However, an ionized molecule may occur in the vicinity of an acceptor in a spherical layer between r_μ and $r_{\mu-\Delta_m}$. In this case, a 1-complex (a negatively charged acceptor plus an ion-

ized molecule) rather than 0-complex will form. Consequently, the concentration N_0 will be lower than in the absence of the overlap.

Thus, the switching-on of the overlap violates the neutrality condition (2): the left-hand side decreases, and the right-hand side increases. The equality will be restored through an increase of μ . (From physical considerations, it is clear that, with increasing μ , the number of negatively charged complexes increases and the number of positively charged complexes decreases.)

3. It is easy to estimate the value of μ from the above. To do this, let us replace all neutral centers by molecules and suppose that $\Delta(\rho) = \Delta_m$ for all molecules. Then, we may apply the impurity band theory for small K to noninteracting molecules. As a result, instead of the equality $\mu = \varepsilon_N$, we obtain $\mu - \Delta_m = \varepsilon_N$. Thus, $\mu < \varepsilon_N + \Delta_m$.

4. Let us crudely estimate, as applied to Si : B (*p*-type), the values of N and N_K at which molecules affect μ . We start from the determination of the lower bound by N , N_{\min} . First, we found N_0 with regard to molecules. For simplicity, we will consider that $\Delta(\rho) = \Delta_m$ for all molecules and that the center-to-center distance lies within the range $(\bar{\rho} \pm 0.5\delta\rho)$, where $\bar{\rho} = 4a_0$ and $\delta\rho = 2a_0$. Under this assumption, the product $\Delta_m\delta\rho$ approximately equals the area under curve (Fig. 3). A certain reason for such a choice is the fact that it is the area under curve that determines the number of molecules in the layer at $\delta\rho < \bar{\rho}$ and $\Delta_m \ll \mu$ (see below). It is easy to see that $\bar{\rho} \ll r_\mu$. Therefore, we will consider molecules as points.

At $(\bar{\rho})^3 \ll (\bar{\rho})^3$, the concentration of molecules is

$$M = (1/2) \times 4\pi N^2 (\bar{\rho})^2 \delta\rho. \quad (4)$$

Note that the inequalities $N_K \ll M \ll N$ are obeyed in our samples. The number of pairs in the layer $(r_\mu, r_{\mu-\Delta_m})$ is $v' = (4\pi/3)M(r_{\mu-\Delta_m}^3 - r_\mu^3)$. To calculate N_0 in the presence of molecules, expression (3) should be multiplied by the probability that the layer $\exp(-v')$ contains no molecule:

$$N_0 = N_K \exp(-v - v'). \quad (5)$$

The right-hand side of equation (2) should be supplemented by the concentrations of 2-complexes containing one or two molecules; these terms are of orders v'/v and $(v'/v)^2$, respectively. At $N = N_{\min}$, the ratio v'/v is small, and these terms may be omitted. However, generally speaking, the quantity v' cannot be omitted in the exponent (2). Thus, as N increases, the contribution of molecules should be taken into account primarily in the calculation of N_0 ($M \sim N^2$). Assuming that $v' \sim 1$ at $N = N_{\min}$, we obtain $N_{\min} \approx 4 \times 10^{15} \text{ cm}^{-3}$. To obtain this estimation, it should be assumed that $\mu = \varepsilon_N$ and taken into

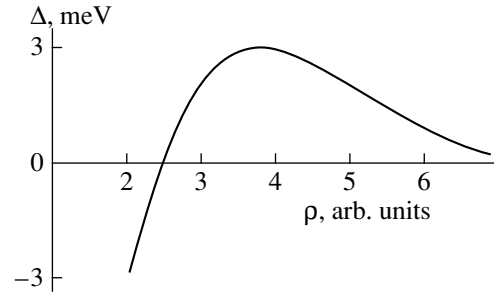


Fig. 3. Dependence of the change in the first ionization energy of an impurity molecule on the center-to-center distances.

account that, under this condition, $(4\pi N/3)r_\mu^3 = z^3$ and $z = (1.63)^3$ [1].

Fluctuations of the potential shield the field of the acceptor at a distance [1]

$$r_s = 0.58 N_K^{-1/2} N^{1/6} \approx (N/N_K)^{1/2} \bar{r}. \quad (6)$$

A molecule that resides in the layer $(r_\mu, r_{\mu-\Delta_m})$ can be ionized if $r_s \gg r_{\mu-\Delta_m}$. Assuming for estimation that $r_s \geq 10r_{\mu-\Delta_m}$, we obtain that the effect of pairs in our samples must become appreciable at $N_K/N = K \leq K_{\max} \leq 10^{-2}$, which is reasonably consistent with the experimental data (see Fig. 1).

The concentration N at which the approximation of isolated molecules is valid is bounded from the above $N < N_{\max}$. Actually, at sufficiently large N , the effect of the third nearest neighboring neutral center separated by a distance $r \gg \bar{\rho}$ from the molecule should be taken into account. The interaction of the center with a neutral molecule can be neglected. The interaction energy $\delta\varepsilon$ of the third center with the electron of an ionized molecule can be estimated [4] at $\delta\varepsilon(r) = e^2 a_0^3 / (2\kappa^2 r^4)$ (the polarizability of a neutral center $\approx a_0^3$). The effect of the third center can be neglected if $\delta\varepsilon(r) \ll \Delta_m$. We determine the critical value $r = r_c$ by the condition $\delta\varepsilon(r_c) = 0.1\Delta_m$. The model of isolated molecules is applicable if the probability $\exp(-(4\pi/3)Nr_c^3)$ that the sphere of radius r_c around the molecule contains no center is close to unity. From here, using the r_c value defined above, we obtain $N < N_{\max} \approx 10^{17} \text{ cm}^{-3}$. The experimental upper bound, as was mentioned above, is close to this value.

5. Thus, the model that takes into account the effect of the interaction of neutral centers on the energy distribution of states provides a complete qualitative explanation of experimental results. This model gives estimations for N_{\min} , N_{\max} , and K_{\max} . Among these values, N_{\max} and K_{\max} are observed experimentally. As to

the lower bound N_{\min} , its existence cannot be verified experimentally, because the conductivity is too small at such small N .

We emphasize once again that our estimates are rather approximate. In this connection, note that the rightfulness of using the light-hole radius $a_0 = 23 \times 10^{-8}$ cm, which determines the overlap of wave functions, is far from evident. Nevertheless, the estimates of N_{\max} and K_{\max} are in a reasonable agreement with the experimental values.

In conclusion, we are to make two comments. The discrepancy between the classical theory and experiment for the samples under discussion relates not only to the ϵ_3 values. A radical disagreement is also observed for the dependence on E and on the magnetic field H . Thus, as E increases, a decrease in σ_3 with E is observed not only at high T (in the region of σ_3 depletion [5]) but in the entire range of T ; depending on T and E , a magnetic field H leads to either a gigantic increase in σ_3 (by a factor of 2–2.5 [6]) or a significant drop (by a factor of 2–3) even at values negligibly small for silicon ($H \approx 15$ kOe). These results call for a special consideration.

At an even smaller compensation $K \leq 5 \times 10^{-4}$, even higher values of ϵ_3 are observed (see Fig. 1). These values exceed the upper bound obtained for ϵ_3 in the approximation of two-center molecules. We believe that this fact is associated with molecules of three and more centers. The probability of the formation of such molecules is small. Therefore, their effect is revealed at smaller N_K . Note in this connection that the first ioniza-

tion energy of three hydrogen atoms separated from each other by distances of order several Bohr radii in various configurations turns out to be considerably lower than the first ionization energy of an isolated hydrogen atom (to 0.4 Ry at $R/a_0 \approx 1.5$ [7]).

The authors are grateful to Ya.E. Pokrovskii for the possibility of performing experiments on sets of samples with transmutation doping.

This work was supported by the Russian Foundation for Basic Research, project no. 98-02-116903.

REFERENCES

1. B. I. Shklovskii and A. L. Éfros, *Electronic Properties of Doped Semiconductors* (Nauka, Moscow, 1979).
2. J. C. Slater, *Quantum theory of molecules and solids*, vol. 1: *Electronic structure of molecules* (McGraw-Hill, New York, 1963).
3. E. M. Gershenson, Yu. A. Gurvich, A. P. Mel'nikov, *et al.*, *Pis'ma Zh. Éksp. Teor. Fiz.* **51**, 204 (1990) [JETP Lett. **51**, 231 (1990)].
4. L. D. Landau and E. M. Lifshits, *Quantum Mechanics* (Nauka, Moscow, 1974).
5. D. I. Aladashvili, Z. A. Adamiya, K. G. Lavdovskii, *et al.*, *Pis'ma Zh. Éksp. Teor. Fiz.* **47**, 390 (1988) [JETP Lett. **47**, 466 (1988)].
6. E. M. Gershenson, Yu. A. Gurvich, A. P. Mel'nikov, *et al.*, *Pis'ma Zh. Éksp. Teor. Fiz.* **54**, 639 (1991) [JETP Lett. **54**, 646 (1991)].
7. H. Conroy and B. Bruner, *J. Chem. Phys.* **40**, 603 (1964).

Translated by A. Bagatur'yants

CONDENSED
MATTER

Anomalous Surface Deceleration of a Domain Wall in an Amorphous Ferromagnet

V. E. Zubov, A. D. Kudakov,¹ and T. S. Fedulova

Moscow State University, Vorob'evy gory, Moscow, 119899 Russia

Received December 1, 1999

Abstract—On soft magnetic amorphous specimens, a rapid decrease in the surface amplitude of 180° domain wall oscillations relative to the bulk amplitude is observed with increasing frequency of the magnetizing field. The dynamics of the domain wall is studied by a magneto-optical method at the specimen surface and by the induction method in the bulk. The results of the experiment disagree with the theory, which takes into account the effect of eddy currents and predicts that, with increasing frequency, the surface amplitude of the domain wall oscillations should decrease slower than the bulk amplitude. The observed behavior of the domain wall is explained by its interaction with macroscopic defects at the specimen surface. This interaction gives rise to unsteady chaotic surface wall displacements, which lead to an increase by several orders of magnitude in the effective surface damping parameter in the Landau–Lifshits equation. © 2000 MAIK “Nauka/Interperiodica”.

PACS numbers: 75.60.Ch, 75.50.Kj

According to the theory developed by a number of authors (see, e.g., [1]), the effect of eddy currents should lead to changes in the shape of a moving domain wall (DW) in a ferromagnetic material. The density of eddy currents caused by the DW motion is lower near the surface and higher in the bulk of the specimen; therefore, in the bulk, the deceleration of the DW due to the eddy currents should be more substantial than at the surface. Thus, the surface amplitude of the DW oscillations in an alternating magnetic field should be higher than the bulk one, and the difference between these amplitudes should increase with increasing frequency of magnetic field. This effect was observed experimentally in iron silicide [2, 3].

In the studies of the oscillations of 180° DW in iron whiskers, which are specimens with a nearly perfect crystal structure both in the bulk and at the surface, a different result was obtained [4]. It was found that, with increasing frequency, the surface amplitude of the DW oscillations in iron whiskers decreased much more rapidly than the bulk one. The experiment showed that such an anomalous behavior of the DW is a result of the physical adsorption of air molecules at the surface of iron crystals [4]. The adsorption causes an increase in the magnetic defect density and, hence, an increase in the effective deceleration of the DW at the surface.

This paper presents a study of the oscillations of 180° DW both at the surface and in the bulk of the specimens of an amorphous ferromagnet, i.e., a material characterized by the most disordered structure. The amorphous ferromagnetic specimens of composition FeCuNbSiB were obtained by the spinning method. Before amorphization, the melt was subjected to spe-

cial time–temperature treatment to obtain a uniform distribution of doping elements and, as a result, an improvement of the soft magnetic properties of the alloy [5]. The specimens were 25–30 μm thick, 0.55 mm wide, and 15–20 mm long. In what follows, the specimens and the results of the experiment are described by using the coordinate system with the *x*-axis and *y*-axis being directed along the specimen length and width, and the direction of the *z*-axis corresponding to the shortest dimension, i.e., the specimen thickness. In the middle of each specimen, a 180° DW oriented along the *yz*-plane was formed. The DW divided the specimen into two domains with the magnetization along the *y*-axis. The effective width of the DW at the surface and the coercive force of the DW were determined by the magneto-optic method and proved to be equal to 7 μm and 0.01 Oe, respectively.

The surface properties of the DW were studied by a magneto-optic method with the use of the equatorial Kerr effect. The surface oscillations of the DW were studied by measuring the equatorial Kerr effect caused by the change in the magnetization of part of the specimen in the course of the DW motion. The slit of a photomultiplier tube scanned the surface along the *x*-axis normally to the DW. The magneto-optic signal was observed only in the region of the DW oscillations. The amplitude of the DW oscillations in the bulk of the specimen was determined by the induction method. A displacement of the DW causes a change in the total magnetic flux in the specimen, and this change is proportional to the DW displacement. To obtain a signal proportional to the amplitude of the DW oscillations in the bulk, a small measuring coil was fitted on the specimen and positioned in the immediate vicinity of the region of magneto-optic measurements. The signal

¹ e-mail: kudakov@adk.phys.msu.su

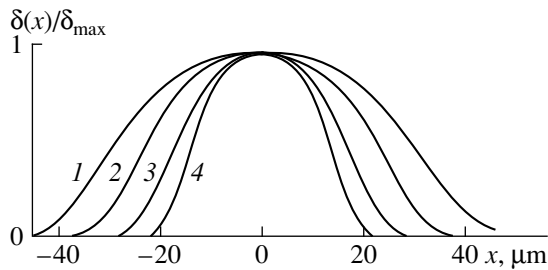


Fig. 1. Distributions of the equatorial Kerr effect, $\delta(x)/\delta_{\max}$, caused by the oscillations of a 180° domain wall in a specimen in an alternating magnetic field with an amplitude of 0.6 Oe; $f = (1)$ 0.02, (2) 2, (3) 10, and (4) 15 kHz.

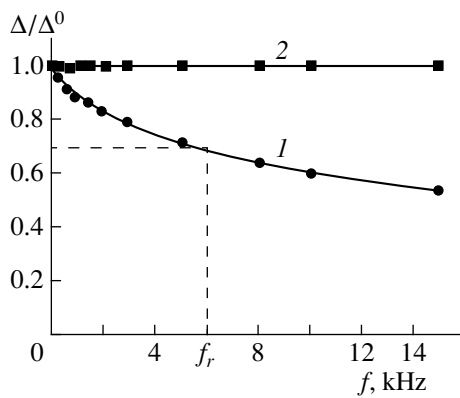


Fig. 2. Frequency characteristics of the amplitude of the domain wall oscillations (1) at the surface and (2) in the bulk of the specimen; f_r is the relaxation frequency for the domain wall oscillations at the surface.

excited in the measuring coil by the external magnetic field was cancelled by an additional coil.

Figure 1 presents the distributions of the equatorial Kerr effect, $\delta(x)/\delta_{\max}$, caused by the magnetization of the domains and observed owing to the oscillations of the DW. The distributions are plotted along the x -axis for a magnetic field of amplitude 0.6 Oe and for different frequencies from 20 Hz to 15 kHz. The peak-to-peak amplitude of the DW oscillations at the surface is determined as the width of the equatorial Kerr effect curve at its base minus the width of the DW [4]. Figure 2 presents the dependence of Δ_s/Δ_s^0 on frequency (curve 1), where Δ_s is the amplitude of the DW oscillations and $\Delta_s^0 = \Delta_s$ at $f \rightarrow 0$. From this figure, it follows that the relaxation frequency (f_r), which corresponds to a 30% decrease in the amplitude of the DW oscillations relative to Δ_s^0 , is about 6 kHz (see Fig. 2). The measurements showed that, in the frequency range from 20 Hz to 15 kHz, the amplitude of the DW oscillations in the bulk (Δ_b) is invariant.

The results obtained in our experiments disagree with the theoretical predictions based on taking into account the effect of eddy currents and testify that the effective deceleration experienced by a moving DW in the near-surface region far exceeds that in the bulk.

The frequency dependences of the amplitude of the 180° DW oscillations observed both at the surface and in the bulk of amorphous magnetic specimens qualitatively agree with the corresponding dependences obtained for single-crystal iron whiskers for which the enhanced surface deceleration of the DW is caused by the formation of surface defects due to the adsorption of air molecules. Therefore, it would appear reasonable to assume that the enhanced surface deceleration of DW in amorphous specimens is also caused by some surface defects. The fast cooling of the melt used for the preparation of amorphous specimens leads to the formation of a microrelief at the specimen surface as well as a macrorelief visible to the unaided eye. Another specific feature of the specimens is that the width of the DW observed in amorphous specimens is an order of magnitude greater than that observed in iron, and it is of macroscopic dimensions. It is well known that a DW most strongly interacts with the crystal defects whose dimensions are close to the DW width [6]. Therefore, the enhanced deceleration of the DW in amorphous specimens can be explained by the interaction of the DW with macroscopic surface defects.

The disagreement between the results of our experiments and the theoretical predictions (see [1]) can be explained by taking into account the mechanism of the anomalously high energy loss experienced by a moving DW in the near-surface region [7]. The mechanism consists of an unsteady chaotic motion of the near-surface part of the DW, this motion being initiated by the surface defects of the specimen. The effective surface damping parameter involved in the Landau–Lifshits equation and determined on the basis of the developed theory proves to be several orders of magnitude higher than the corresponding parameter for the specimen bulk, which explains the enhanced surface deceleration of the DW. The unsteady chaotic displacements of the DW cause an increase in the eddy current density in the surface region, which leads to an additional deceleration of the DW. On the basis of the mechanism of the unsteady surface displacements of the DW, one also can explain the results obtained in the experiments with iron silicide [2, 3]. Such an explanation is supported by the fact that, in one of these experiments [3], the surface amplitude of the DW oscillations was much less than the amplitude predicted by the theory on the basis of effect of eddy currents, while, in the other experiment [2], the dynamical bowing of the DW was found to depend on the amount of defects in the specimens. In addition, in both these experiments [2, 3], an unsteady motion of the DW at the specimen surface was observed.

We are grateful to V.S. Tsepelev for supplying us with the amorphous magnetic specimens.

This work was supported by the Russian Foundation for Basic Research (grant no. 97-03-32409a) and a grant from the Ministry of Education of the Russian Federation (the St. Petersburg Competition Center).

REFERENCES

1. B. N. Filippov and A. P. Tankeev, *Dynamical Effects in Ferromagnets with Domain Structure* (Nauka, Moscow, 1987).
2. N. K. Esina, V. F. Tiunov, and V. A. Zaikova, *Fiz. Met. Metalloved.* **53**, 281 (1982).
3. M. Celasco, A. Masoero, P. Mazzetti, *et al.*, *IEEE Trans. Magn.* **MAG-22**, 502 (1986).
4. V. E. Zubov, A. D. Kudakov, N. L. Levshin, *et al.*, *J. Magn. Magn. Mater.* **140-144**, 1895 (1995).
5. Yu. N. Starodubtsev, L. D. Son, V. S. Tsepelev, *et al.*, *Rasplavy* **4**, 76 (1992).
6. G. S. Krinchik, *Physics of Magnetic Phenomena* (Mosk. Gos. Univ., Moscow, 1985).
7. V. E. Zubov, A. D. Kudakov, N. L. Levshin, *et al.*, *Proceedings of Moscow International Symposium on Magnetism, Moscow, 1999*, Part 1, p. 61.

Translated by E. Golyamina

CONDENSED
MATTER

Polarization Anomalies in a Relaxor Ferroelectric

V. V. Gladkii*, V. A. Kirikov*, S. V. Nekhlyudov*, T. R. Volk*, and L. I. Ivleva**

* *Shubnikov Institute of Crystallography, Russian Academy of Sciences, Moscow, 117333 Russia*

** *General Physics Institute, Russian Academy of Sciences, Moscow, 117942 Russia*

Received December 2, 1999

Abstract—With a strontium barium niobate crystal used as an example, it is experimentally demonstrated that relaxor ferroelectrics exhibit pronounced polarization anomalies, which manifest themselves in the difference between the trajectories of the dielectric hysteresis observed in several repeated cycles of a varying external electric field. These anomalies originate from the nonuniformity of the relaxor composition, local symmetry lowering, local internal electric field, and a wide distribution of potential barriers in energy for the polarized regions. The anomalies can be observed only in slowly varying (quasistatic) or constant electric fields.
© 2000 MAIK “Nauka/Interperiodica”.

PACS numbers: 77.80.Fm, 77.22.Ej

Relaxor ferroelectrics include a large group of solid solutions with a perovskite or tungsten bronze structure. In contrast to ordinary ferroelectrics whose physical properties are adequately described by the Landau–Ginzburg–Devonshire theory, relaxors possess the following specific features [1]. They have a disordered structure, because some ions can occupy different positions, and the chemical composition of a relaxor varies over the crystal volume. Because of the composition fluctuations, the phase transition from nonpolar to polar state and the anomalies of the physical properties are spread over a wide temperature range called Curie region. In this region, the inhomogeneous macroscopic structure consists of a nonpolar matrix containing small-size polar regions ~ 100 Å (nanodomains), the dielectric permittivity exhibits a weak spread maximum at some temperature T_m , as well as a dispersion at low radio frequencies, and the dielectric hysteresis loop slowly degrades with heating above T_m [2]. In properties and structure, relaxors are similar to ferroelectrics at temperatures well below the Curie region and to dielectrics at temperatures above this region. The piezoelectric, pyroelectric, and electrooptic characteristics of relaxors are characterized by high values and high nonlinearity. Relaxor ferroelectrics show considerable promise for the applications in piezoelectric technology, electronics, nonlinear optics [1], and holography [3].

The dielectric properties of relaxors had usually been studied in alternating electric fields of frequency ~ 100 Hz [1, 2]. This paper presents the results obtained by measuring the polarization P in a slowly varying (quasistatic) electric field E , which made it possible to study the evolution of long-lived metastable states in this type of crystals.

The measurements were performed by precision electrometry using an equal-arm bridge with a voltage

sensitivity of 20 μV and an electric charge sensitivity of 4×10^{-6} μC . The voltage compensation in the bridge diagonal was performed with the help of an IBM PC and controlled peripheral units in steps of 0.15 mV. The polarization P was continuously recorded in the real-time mode and could be observed on the display of a PC [4]. The electric field E was generated by a B5-50 voltage source with the output voltage within 0 – 300 V, with a varied polarity. The voltage source was controlled by a programmed unit. The experimental setup allowed one to measure several successive cycles of the specimen repolarization with a step being a multiple of 1 V and a time interval being a multiple of 1 s. The maximum number of steps was 1200 . The magnitude of the step in voltage, the step duration, and the maximum voltage magnitude could be varied in the course of the experiment.

For our studies, we selected a $\text{Sr}_{0.61}\text{Ba}_{0.39}\text{Nb}_2\text{O}_6$ (SBN) single crystal doped with 0.44 mol % La and 0.023 mol % Ce. The crystal was grown by the Czochralski method at the General Physics Institute of the Russian Academy of Sciences [5]. The introduction of Ce was necessary for the concurrent studies of photorefractive effects in this crystal as a promising material for dynamical holography [3]. Among all known materials of this kind, the selected crystal has the lowest temperature corresponding to the maximum dielectric permittivity: $T_m = 37^\circ\text{C}$. Therefore, in this crystal, the anomalous behavior of P , which is expected in relaxors near T_m , can be more easily observed by electrometry owing to the relatively high resistance: $\sim 10^{13}$ Ω at 0°C .

The specimens were grinded plates of polar Z-cuts of the crystal with the dimensions $2.5 \times 3 \times 0.7$ mm. The larger faces were covered with silver paint. The temperature of the specimen was stabilized in a constant-temperature cabinet to an accuracy of no lower

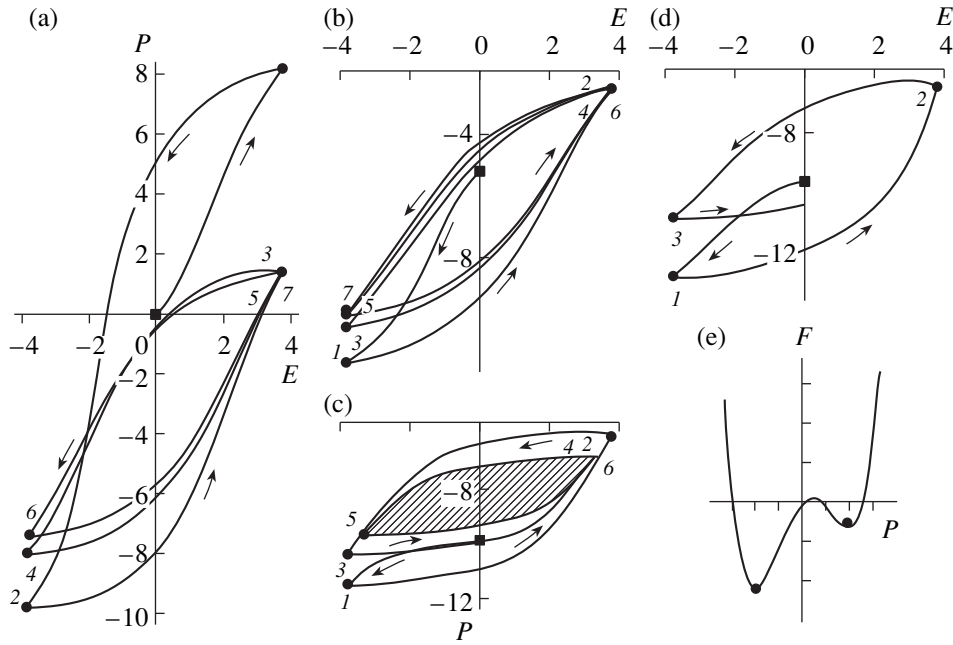


Fig. 1. Hysteresis loops in the dependence of the polarization P ($\mu\text{C}/\text{cm}^2$) on the electric field E (V/cm) for an SBN crystal at $T =$ (a, b) 274, (c) 250, and (d) 236 K; (e) schematic representation of the local free energy F as a function of the polarization P .

than 0.03 K. Prior to every measurement run, the specimen was heated above T_m and then cooled to the given temperature.

Figure 1 presents the quasistatic loops of the dielectric hysteresis observed in the dependence of P on E in several repeated cycles of the field variation at three different temperatures. The duration of one cycle is 1 h. The beginning of the repolarization process is indicated by black squares. The first loop (Fig. 1a) corresponds to the case of opposite directions of the polarization P induced by the field E at the beginning of the process and the initial polarization P_0 (unipolarity) ($P_0 < 0$); the other three loops (Figs. 1b–1d) correspond to the case of coincident directions of these polarizations. In contrast to the loop of an ordinary homogeneous ferroelectric, these loops have a common specific feature, namely, the difference between the values of P at the beginning and at the end of a complete cycle of the electric field variation and the difference between the trajectories of P in different cycles. The boundary values of P reached at the maximum fields $E = \pm E_{\text{max}}$ are indicated in the figure by black circles, and their sequence in time is shown by numbers. This specific feature is most pronounced for the first cycles. As the cycles are repeated many times, the trajectories of P approach each other and merge into one common loop, so that the loops take their usual form observed in the case of fast multiple periodic variations of E [2]. This process is accompanied by a considerable decrease in the amplitude of P and a displacement of the loop toward nonzero values of P , which is an indication of the unipolarity peculiar to the specimen in the state of

equilibrium. As the temperature is reduced, the amplitude of P decreases, and the width of the loop and the unipolarity are increased. With a decrease in the amplitude of E , the amplitude of P also decreases, but the form of the loop remains virtually unchanged (the shaded region in Fig. 1c).

The specific features of the quasistatic hysteresis loops obtained for the crystal under study can be easily explained, and presumably, they can serve as a direct verification of the existing concepts of the macroscopic polar structure of relaxors. The random distribution of Sr in two nonequivalent cation positions [1] should give rise to a gradient of their concentration as well as to a local symmetry lowering and an internal electric field E_i . As a result, the local free energy $F = -\alpha P^2 + \beta P^4 - (E_i + E)p$ should be an asymmetric two-minimum function of P [2]. Since the direction and magnitude of E_i are random variables, the depths of the minima are also random variables. Figure 1e shows an example of the local free energy F for the case $E_i < 0$. At $E_i > 0$, the positions of the deep and shallow minima are interchanged. If the directions of the internal field E_i and the external field E coincide, the height of the barriers separating the shallow minima from the deep ones is reduced and the process of polarization from the local metastable states to the stable ones is accelerated. If the directions of E_i and E are opposite, this process is decelerated and the reverse polarization begins at $|E| > |E_i|$. In a field E with alternating sign, a total repolarization of the whole crystal is possible only when the condition $|E| > |E_i|$ holds within the entire crystal volume. Evidently, in the SBN crystal under study, the follow-

ing situation takes place. The metastable and stable states are, firstly, long-lived ones because of the high barriers separating them; secondly, the lifetimes of these states are distributed over a wide range of values. As a result, at $E = 0$, the crystal remains for a long time in a mixed state with part of the crystal being metastable and the other part being stable. The field E of both signs converts some regions of the crystal to the stable states with $P > 0$ and $P < 0$. The volume of these regions increases with increasing E . At the same amplitudes of E , an inverse transition of these regions to the initial states is practically impossible because of the high barriers. Therefore, these regions do not participate in the following repolarization process, and only the lesser part of the regions, i.e., the regions where $|E| > |E_c|$, contribute to the repolarization. As a result, the dielectric hysteresis loops take the anomalous form shown in Fig. 1. The measure of the relative volume of the regions that do not take part in the following repolarization can be the difference between the polarization values at the end of the cycle of the electric field variation (e.g., the difference in P between points 1 and 3 of the first cycle). As the temperature of the crystal decreases, all barriers grow; hence, at the same field amplitude, the relative volume of the regions taking part in the repolarization process decreases. If the temperature of the crystal increases, the barriers become lower and the stable polarized state of the crystal is easily erased.

More information on the heights of the barriers and their distribution in energy can be derived from the measurements of the relaxation of the polarization P that occurs when a constant external electric field E is abruptly turned on and off. The results of our preliminary experiments offer the following conclusions. At any value of E below or above the half-width of the loop, the polarization variation ΔP first occurs as a jump (an above-barrier process without a distinct coercive field) and then by the thermal activation mechanism obeying the universal power law $\Delta P \sim (1 + t/a)^n$, where t is time and a and n are parameters depending on E and temperature (as in the case of ordinary ferroelectrics). From the measured $\Delta P(t)$, one can determine the equilibrium polarization P_e and, in the framework of the model with independent relaxation centers, reconstruct the continuous spectrum characterizing the distribution of barriers in energy [4]. In ordinary ferro-

electrics, the polarization P relaxes to the value $P_e = P_s = \text{const}$ at any low electric field E , and, when the field E is turned off, the polarization relaxes to $P_e = 0$ [1]. In an SBN crystal, in the Curie region, we always have $P_e \neq \text{const}$, and the value of this quantity is the greater the higher the electric field E in both polarization and depolarization processes. Such a dependence should be retained up to some critical field corresponding to the polarization saturation, this field being presumably fairly high. As the temperature increases, the spectra characterizing the distribution of barriers in energy are shifted toward lower energy values, while the jump ΔP and the equilibrium polarization P_e are decreased. According to our data, the relaxation times of the polarization P in SBN are about 1 min and over. No wonder that the anomalies of polarization observed in our experiments could not manifest themselves in alternating electric fields of frequency ~ 100 Hz [2].

The data presented above testify that, in the wide Curie region, the SBN crystals are strictly speaking no ferroelectrics, because they have no definite values of coercive field and equilibrium polarization. Presumably, similar specific features of polarization are characteristic of all compounds called relaxor ferroelectrics and providing an example of a clearly defined nonergodic system.

This work was supported by the Russian Foundation for Basic Research (project no. 99-02-17303).

REFERENCES

1. M. E. Lines and A. M. Glass, *Principles and Application of Ferroelectrics and Related Materials* (Clarendon, Oxford, 1977; Mir, Moscow, 1981).
2. L. E. Cross, *Ferroelectrics* **76**, 241 (1987).
3. F. Micheron, C. Mayeux, and J. C. Trotier, *Appl. Opt.* **13**, 784 (1974).
4. V. V. Gladkiĭ, V. A. Kirikov, S. V. Nekhlyudova, *et al.*, *Fiz. Tverd. Tela* **39**, 2046 (1997) [*Phys. Solid State* **39**, 1829 (1997)].
5. L. I. Ivleva, N. V. Bogodaev, N. M. Polozko, *et al.*, *Opt. Mater.* **4**, 168 (1995).

Translated by E. Golyamina

CONDENSED
MATTER

Magnetoresistance of a Two-Dimensional Electron Gas in a Parallel Magnetic Field¹

V. T. Dolgoplov* and A. Gold**

*Institute of Solid-State Physics, Russian Academy of Sciences, Chernogolovka, Moscow oblast, 142432 Russia

** Centre d'Elaboration de Matériaux et d'Etudes Structurales (CNRS), 31055 Toulouse, France

Received November 4, 1999; in final form, December 7, 1999

Abstract—The conductivity of a two-dimensional electron gas in a parallel magnetic field is calculated. We take into account the magnetic-field-induced spin-splitting, which changes the density of states, the Fermi momentum, and the screening behavior of the electron gas. For impurity scattering, we predict a positive magnetoresistance for low electron density and a negative magnetoresistance for high electron density. The theory is in qualitative agreement with recent experimental results found for Si inversion layers and Si quantum wells.
© 2000 MAIK “Nauka/Interperiodica”.

PACS numbers: 73.50.Jt, 71.30.+h

In recent experiments [1–9], the transport properties of the two-dimensional electron gas (2D EG) in Silicon inversion layers and GaAs heterostructures have been studied by applying a parallel magnetic field. The motivation to study transport properties came from a renewed interest into the metal-insulator transition in a 2D EG [10–12]. In the experiments, a strong positive magnetoresistance has been found in the metallic phase. The experimental fact that the magnetoresistance saturates above the magnetic field B_c , corresponding to a totally polarized electron system, was interpreted as a manifestation for the importance of the spin-polarization [8, 9]. At electron densities where a strong magnetoresistance is found, it was shown experimentally that the conductivity increased with decreasing temperature [5, 9, 13, 14]. This temperature dependence was successfully described by a temperature dependant screening behavior [15–17].

One expects that the transport properties of the metallic phase of a 2D EG, depending on temperature and magnetic field, are explained in the frame of a single theory. For a weakly disordered EG, we propose in the present paper an explanation of the large magnetoresistance in the metallic phase due to the magnetic field induced changes of the screening properties of the 2D EG. The corresponding temperature dependence is also described. The effect of the parallel magnetic field is to provide the spin-polarization of the EG. In the fully polarized system, the spin degeneracy is lifted and the Fermi energy increases by a factor two together with a reduction of the density of states by a factor two compared to the two-dimensional EG in zero magnetic field. In fact, we shall show that these ingredients are already sufficient to describe a positive

magnetoresistance at low and intermediate electron density and a negative magnetoresistance at high electron density.

We use a minimal model in order to describe the effects of the parallel magnetic field. The term parallel means that the magnetic field is in the plane of the EG. First, we assume that the two-dimensional EG has zero width in the direction perpendicular to the interface. Second, we consider only charged impurity scattering without spin-flip processes. Screening effects are taken into account within the random-phase approximation including many-body effects described by the local-field correction.

The electron density N defines the Fermi wave number k_F of the 2D EG via $N = g_s g_v k_F^2 / 4\pi$. Here, g_v and g_s are the valley and the spin degeneracy factors, respectively, and k_F is the Fermi wave number. The Fermi energy $\epsilon_F = k_F^2 / 2m^*$ is given by the Fermi wave number and the effective mass m^* . For Si inversion layers and Si quantum wells, $g_v = 2$, while for GaAs/AlGaAs heterostructures the valley degeneracy factor is $g_v = 1$. For zero field, the spin degeneracy is $g_s = 2$, while for large magnetic field the degeneracy factor is given by $g_s = 1$. For intermediate fields, the system is partially spin-polarized. We assume that the disorder is due to charged impurities of density N_i located in the plane of the EG. The magnetic field applied parallel to the 2D EG plane leads to a Zeeman energy $\Delta E = \pm g^* \mu_B B / 2$. Here g^* is the effective Landé g -factor. The system will be total spin-polarized if ΔE is larger than ϵ_F . This condition defines a critical magnetic field B_c for complete spin-polarization and given by $B_c = 2\epsilon_F / g^* \mu_B$.

¹ This article was submitted by the authors in English.

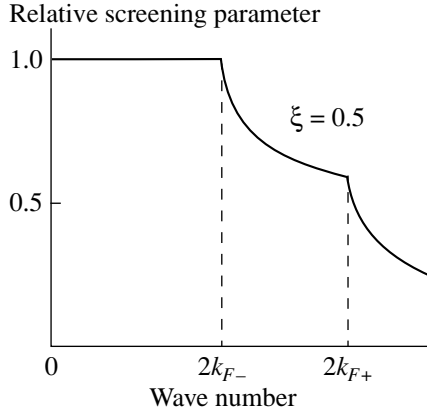


Fig. 1. Effective screening parameter for the partially spin-polarized 2D EG as function of the wave number.

For charged impurity scattering, the scattering time τ is given by [16, 18]

$$\frac{h}{\tau} = \frac{(2\pi)^2}{g_s g_v} \frac{N_i}{N} \frac{1}{[1 - (G(2k_F, g_s) + 2k_F/q_s)]^2}. \quad (1)$$

Here, $G(2k_F, g_s)$ is the local-field correction which describes many-body effects and depends on the spin degeneracy. Within the random-phase approximation, the local-field correction $G(2k_F, g_s) = 0$ is neglected. Most important is that the Fermi wave number $k_F = (4\pi N/g_s g_v)^{1/2}$, the screening wave number $q_s = g_s g_v / a^*$, and the Fermi energy $\epsilon_F \propto k_F^2 \propto 1/g_s g_v$ depend on the spin degeneracy.

In fact, there are three factors which are important for the scattering time: (i) the density of states ρ_F at the Fermi energy, which leads to $1/\tau \propto \rho_F \propto g_s$; (ii) the Fermi wave number (due to backscattering processes up to $2k_F$) with $k_F \propto 1/g_s^{1/2}$; and (iii) the screening wave number $q_s \propto g_s$, which enters, together with $2k_F$, the screening function $\epsilon(q)$ and contributes as $1/\epsilon^2(q=2k_F) \propto 1/(1 + q_s/2k_F)^2$, which leads for $q_s \gg 2k_F$ (low density) to $[1/\epsilon(q=2k_F)]^2 \propto 1/g_s^3$ and for $q_s \ll 2k_F$ (high density) to $[1/\epsilon(q=2k_F)]^2 = 1$. Consequently, for $q_s \gg 2k_F$ the conductivity, σ is given by $\sigma \propto g_s^2$, and for $q_s \ll 2k_F$ one finds $\sigma \propto 1/g_s$. We conclude that, for $q_s \gg 2k_F$, the resistivity ρ increases with increasing field $\rho(B=B_c)/\rho(B=0) = 4$, while for $q_s \ll 2k_F$ the resistivity decreases with increasing field $\rho(B=B_c)/\rho(B=0) = 0.5$.

We introduce the partially spin-polarized 2D EG by the densities N_{\pm} given by $N_{\pm} = N(1 \pm \xi)/2$, where the spin-polarization parameter is $\xi = (N_+ - N_-)/N$ with $0 \leq \xi \leq 1$. In terms of the magnetic field, the polarization parameter is given by $\xi = g^* m_B B / 2\epsilon_F$. For the partially spin-polarized system, we argue as follows: qualitatively the spin-polarization leads to different

k_F -vectors for spin-up [$k_{F+} = k_F(1 + \xi)^{1/2}$] and spin-down [$k_{F-} = k_F(1 - \xi)^{1/2}$] electrons (or holes). The effective screening parameter [18] for finite spin-polarization as a function of the wave number is shown in Fig. 1. Note that, for $k_{F-} \leq q \leq k_{F+}$, the screening parameter is strongly wave-number dependent. By taking into account this effective screening parameter for the partially polarized electron gas, we get for the conductivity in the case of $q_s \gg 2k_F$ a positive magnetoresistance

$$\frac{\sigma(0 \leq B \leq B_c)}{\sigma(B=0)} = \frac{1 - \xi}{2} + \frac{\pi(1 + \xi)}{16f(v)}, \quad (2)$$

with

$$f(v) = \arcsin(v)/4 + [\pi/2 - \arcsin(v)]/[2 - (1 - v^2)^{1/2}]^2, \quad (3)$$

and

$$v = [(1 - \xi)/(1 + \xi)]^{1/2}. \quad (4)$$

The function $f(v)$ has the correct limits $f(v=0) = \pi/2$, which implies $\rho(B=0)/\rho(B=0) = 1$, and $f(v=1) = \pi/8$, which implies $\rho(B=B_c)/\rho(B=0) = 4$.

In Si inversion systems, the electron density corresponding to $q_s = 2k_F$ is quite high: $N = 2.8 \times 10^{13} \text{ cm}^{-2}$. In GaAs the density corresponding to $q_s = 2k_F$ is much lower: $N = 1.6 \times 10^{11} \text{ cm}^{-2}$. We obtain for $q_s \ll 2k_{F-}$ a negative magnetoresistance:

$$\frac{\sigma(0 \leq B \leq B_c)}{\sigma(B=0)} = 1 + \xi^2. \quad (5)$$

We mention that the predicted magnetoresistance is insensitive to the angle between the electric current and the magnetic field in the 2D EG plane. This fact allows one to separate the magnetoresistance caused by spin effects from the magnetoresistance caused by orbital motion in a 2D EG with finite width. The orbital effect was discussed recently and depends on the width of the 2D EG [19].

For the 2D EG, we expect the same increase of the resistance in a magnetic field normal to the 2D EG plane if the magnetic field is smaller than the quantizing one (for instance, $B < 0.4 \text{ T}$ for high mobility Si inversion layers). With the magnetic field normal to the 2D EG plane, the positive magnetoresistance due to the spin will be in competition with the negative magnetoresistance due to weak localization. This means that, for a correct interpretation of the weak localization contribution, it is not enough to compare the resistance values without a field and in a weak normal field, as it is done in the literature. We suggest that spin dependent effects should be measured in a parallel magnetic field and the corresponding correction has to be introduced to describe the magnetoresistance in the normal magnetic field. We expect that the correction due to spin-

polarization has the same order of magnitude as the weak localization contribution.

For the temperature dependence, using our analytical results for charged impurity scattering [16], we predict for $B = 0$ and $B \geq B_c$

$$\sigma(T < \varepsilon_F) = \sigma(T = 0) \times \left[1 - 4 \ln 2 \frac{1 - G(2k_F, g_s)}{1 - G(2k_F, g_s) + 2k_F/q_s} \frac{k_B T}{\varepsilon_F} \right]. \quad (6)$$

Note that, for $g_s = 1$, the Fermi energy increases by a factor 2 compared to $g_s = 2$. Correspondingly, the temperature dependence is weaker for a spin-polarized EG compared to an unpolarized one.

It is not straightforward to apply (1)–(6) to remote doping with a large spacer width α , because one cannot ignore the form factor, which enters the theory [18, 20]. Remote doping is important in GaAs/Al_xGa_{1-x}As heterostructures. For $2k_F\alpha \gg 1$ we predict that the magnetoresistance is always positive and given by $\rho(B \geq B_c)/\rho(B = 0) = 2^{1/2}$ and the linear temperature dependence of the conductivity will disappear due to a form factor, which enters the theory as $\exp(-4\alpha k_F)$ [21]

We briefly discuss the limitations of our approach. We assume a 2D EG with zero thickness in the direction normal to the plane of the EG. Our theory is formulated for weak disorder and low temperature. Therefore, (1)–(6) cannot be applied near the metal-insulator transition and the Fermi energy should exceed the temperature significantly. In silicon inversion layers, interface-roughness scattering is important for intermediate and high electron density [18]. For interface-roughness scattering, we expect the same results as found for impurity scattering.

In (2)–(5), we have ignored many-body effects described by a local-field correction. For a low electron density, where $2k_F/q_s \ll 1$, we get, in fact,

$$\frac{\sigma(B \geq B_c)}{\sigma(B = 0)} = \frac{1 [1 - G(2k_F, g_s = 1)]^2}{4 [1 - G(2k_F, g_s = 2)]^2}. \quad (7)$$

Numerical results concerning $G(2k_F, g_s)$ for $g_s = 2$ and $g_s = 1$ [22] indicate that the magnetoresistance might increase by using a finite local-field correction.

At the present time, detailed experimental results for the conductivity of the good metallic phase in a parallel magnetic field are missing. Below, we compare results of our calculation with some experimental data from the literature. In Fig. 2, we compare curves from (2)–(4) with experimental points obtained from the high-mobility silicon inversion 2D EG of [8]. The agreement between theory and experiment is quite good for the maximal electron density $N = 2.1 \times 10^{11} \text{ cm}^{-2}$. However, for an electron density of $N = 1.7 \times 10^{11} \text{ cm}^{-2}$, the experimental magnetoresistance exceeds the theoretical one nearly twice. We believe that at this density the sample is already close to the metal-insula-

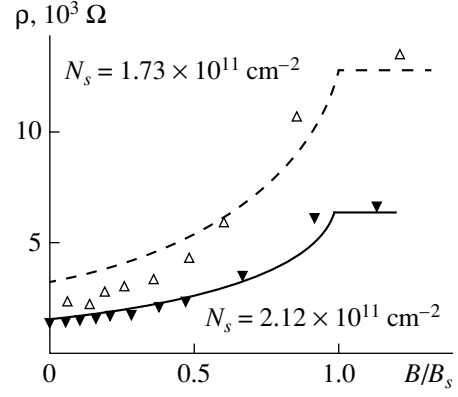


Fig. 2. Resistivity as function of the parallel magnetic field (in units of the critical magnetic field B_c for complete spin-polarization) for parameters corresponding to silicon. The solid points are experimental results [8] for two different electron densities taken from experiments.

tor transition, which occurs for this sample near $N \sim 1 \times 10^{11} \text{ cm}^{-2}$.

The ratio $\rho(B > B_c)/\rho(B)$ found in [3] for the two highest electron densities $N = 2.2 \times 10^{11} \text{ cm}^{-2}$ and $N = 2.6 \times 10^{11} \text{ cm}^{-2}$ is very close to the result of our calculation $\rho(B > B_c)/\rho(B) = 4$.

For $2k_F/q_s \ll 1$, we conclude that the coefficient of the linear temperature dependence in (6) should be $4 \ln 2 = 2.77$ for $B = 0$ and $B > B_c$, independent of the magnetic field. This prediction is in good agreement with experiments [9], where $\rho(T) = \rho(T = 0)[1 + 2.9k_B T/\varepsilon_F]$ was found for Si quantum wells for $B = 0$ and $B > B_c = 9 \text{ T}$. The ratio $\rho(B \geq B_c)/\rho(B = 0) = 2$, also observed in [9], might be explained by a finite spacer effect.

We emphasize that, for $2k_F/q_s \ll 1$, the coefficient of the linear temperature dependence is universal and does not depend on the local-field correction. Such a universal behavior as the function of the carrier density was already verified in experiments with GaAs heterostructures using holes [5].

The crossover point for the transition from a positive magnetoresistance to a negative magnetoresistance is given by $2k_F = q_s$ with $q_s \propto 1/a^*$ and with the corresponding carrier density $N \propto 1/a^{*2}$. With increasing mass, this density increases. Assuming that charged impurities are located in the GaAs, we expect in GaAs/Al_xGa_{1-x}As heterostructures for $N = 3 \times 10^{11} \text{ cm}^{-2}$ a positive magnetoresistance for holes, as already seen in experiment [5], and a negative magnetoresistance for electrons. In conclusion, we presented a theory for the magnetoresistance of a parallel field and for the temperature dependent resistance based on the spin-polarization of the two-dimensional EG. A very important ingredient in our approach is the screening behavior of the spin-polarized system. Recent

experimental results support our theoretical predictions.

This work was supported in part by the Russian Foundation for Basic Research under Grants 97-02-16829 and 98-02-16632 and the program "Nanostructures" from the Russian Ministry of Sciences under Grant 97-1024.

REFERENCES

1. V. T. Dolgoplov, G. V. Kravchenko, A. A. Shaskin, and S. V. Kravchenko, *Pis'ma Zh. Éksp. Teor. Fiz.* **55**, 701 (1992) [*JETP Lett.* **55**, 733 (1992)].
2. D. Simonian, S. V. Kravchenko, M. P. Sarachik, and V. M. Pudalov, *Phys. Rev. Lett.* **79**, 2304 (1997).
3. V. M. Pudalov, G. Brunthaler, A. Prinz, and G. Bauer, *Pis'ma Zh. Éksp. Teor. Fiz.* **65**, 887 (1997) [*JETP Lett.* **65**, 932 (1997)].
4. D. Simonian, S. V. Kravchenko, M. P. Sarachik, and V. M. Pudalov, *Phys. Rev. B* **57**, R9420 (1998).
5. M. Y. Simmons, A. R. Hamilton, M. Pepper *et al.*, *Phys. Rev. Lett.* **80**, 1292 (1998).
6. K. M. Mertes, D. Simonian, M. P. Sarachik *et al.*, *Phys. Rev. B* **60**, R5093 (1999).
7. J. Yoon, C. C. Li, D. Shahar *et al.*, *Phys. Rev. Lett.* **82**, 1744 (1999).
8. T. Okamoto, K. Hosoya, S. Kawaji, and A. Yagi, *Phys. Rev. Lett.* **82**, 3875 (1999).
9. T. Okamoto, K. Hosoya, S. Kawaji *et al.*, *Cond-mat/9906425* (1999).
10. S. V. Kravchenko, G. V. Kravchenko, J. E. Furneaux *et al.*, *Phys. Rev. B* **50**, 8039 (1994).
11. S. V. Kravchenko, W. E. Mason, G. E. Bowker *et al.*, *Phys. Rev. B* **51**, 7038 (1995).
12. S. V. Kravchenko, D. Simonian, M. P. Sarachik *et al.*, *Phys. Rev. Lett.* **77**, 4938 (1996).
13. K. M. Cham and R. G. Wheeler, *Phys. Rev. Lett.* **44**, 1472 (1980).
14. E. A. Vydrov, V. T. Dolgoplov, S. I. Dorozhkin, and N. B. Zhitenev, *Zh. Éksp. Teor. Fiz.* **94**, 234 (1988) [*Sov. Phys. JETP* **67**, 998 (1988)].
15. F. Stern, *Phys. Rev. Lett.* **44**, 1469 (1980).
16. A. Gold and V. T. Dolgoplov, *Phys. Rev. B* **33**, 1076 (1986).
17. S. Das Sarma and E. H. Hwang, *Phys. Rev. Lett.* **83**, 164 (1999).
18. T. Ando, A. B. Fowler, and F. Stern, *Rev. Mod. Phys.* **54**, 437 (1982).
19. S. Das Sarma and E. H. Hwang, *Cond-mat/9909452* (1999).
20. A. Gold, *Phys. Rev. B* **44**, 8818 (1991).
21. A. Gold, *Phys. Rev. B* **41**, 8537 (1990).
22. A. Gold, *Z. Phys. B* **103**, 491 (1997).

Energy Relaxation of Two-Dimensional Electrons in the Quantum Hall Effect Regime

K. V. Smirnov, N. G. Ptitsina, Yu. B. Vakhtomin,¹ A. A. Verevkin,
G. N. Gol'tsman, and E. M. Gershenson

Moscow State Pedagogical University, Moscow, 113567 Russia

Received November 19, 1999

Abstract—The mm-wave spectroscopy with high temporal resolution is used to measure the energy relaxation times τ_e of 2D electrons in GaAs/AlGaAs heterostructures in magnetic fields $B = 0$ –4 T under quasi-equilibrium conditions at $T = 4.2$ K. With increasing B , a considerable increase in τ_e from 0.9 to 25 ns is observed. For high B and low values of the filling factor ν , the energy relaxation rate τ_e^{-1} oscillates. The depth of these oscillations and the positions of maxima depend on the filling factor ν . For $\nu > 5$, the relaxation rate τ_e^{-1} is maximum when the Fermi level lies in the region of the localized states between the Landau levels. For lower values of ν , the relaxation rate τ_e^{-1} is maximum at half-integer values of ν when the Fermi level is coincident with the Landau level. The characteristic features of the dependence $\tau_e^{-1}(B)$ are explained by different contributions of the intra-level and interlevel electron–phonon transitions to the process of the energy relaxation of 2D electrons. © 2000 MAIK “Nauka/Interperiodica”.

PACS numbers: 73.50.Jt, 73.40.Hm

1. In the last decade, the electron–phonon interaction and the mechanisms of the energy relaxation of hot carriers were one of the most important problems of the physics of 2D structures. For the case of the scattering by acoustic and optical phonons in a wide temperature range in the absence of magnetic field, this problem has been solved by many authors, both theoretically (e.g., [1, 2]) and experimentally (e.g., [3, 4]). For a magnetic field perpendicular to the 2D layer, the electron–phonon interaction becomes essentially different because of the quantization of the carrier energy in the 2D plane.

A number of theoretical publications present the calculation of the energy relaxation rate of electrons in a real situation with allowance for the broadening of the Landau levels, as well as the appearance of a region of delocalized states near the center of the Landau level and localized states between the levels in the electron energy spectrum [5–8]. It was shown that, in a quantizing magnetic field, the spectrum of phonons involved in the interaction with electrons is essentially altered, which should result in a change in the energy relaxation rate.

Because of the dependence of the density of electron states on magnetic field, the energy relaxation rate should experience oscillations similar to the resistance oscillations in the Shubnikov–de Haas effect.

The energy relaxation may occur at the expense of the transitions both between the Landau levels and within them. The conditions of the experiment determine which of these two processes prevails. The object of most experimental studies is the spectrum of phonons involved in the interaction with electrons in magnetic field, as well as their angular distribution [6–9]. The measurements of the Landau level population by magnetic tunneling spectroscopy [10] provided the estimates of the energy relaxation time τ_e for the interlevel electron transitions. In magnetic fields $B \geq 4$ T, this quantity was found to be equal to ≈ 100 ns, which far exceeds the values of τ_e corresponding to zero magnetic field. As for the direct measurements of the energy relaxation times in magnetic field, no such experiments had been described in the literature.

2. We studied the inelastic relaxation of two-dimensional electrons in GaAs/AlGaAs heterostructures at the temperature $T = 4.2$ K in magnetic field 0–4 T perpendicular to the 2D plane. The measurements were performed under the weak heating conditions when the free carriers could be considered as quasi-equilibrium ones. We measured the relaxation time of the mm-wave photoconductivity caused by the nonresonance absorption of electromagnetic radiation in the regime of Shubnikov–de Haas oscillations of the resistance (the energy of the radiation quantum $\hbar\omega = 0.6$ meV was much less than $\hbar\omega_C$ for $B > 1$ T, where ω_C is the cyclotron frequency). For the measurements, we used GaAs/AlGaAs structures with the concentration $n_s \approx$

¹ e-mail: vachtomin@mail.ru

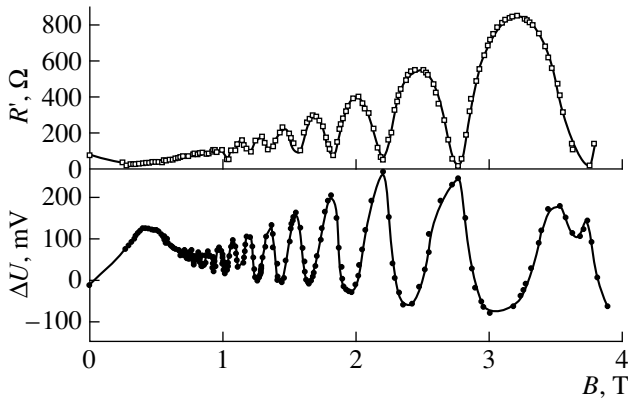


Fig. 1. (●) Photoconductivity signal in the mm-wave range ΔU and (□) the oscillatory contribution to the resistance of the sample R' versus the magnetic field B . $R' = R - \Delta R(B)$, where $\Delta R(B)$ is the contribution of the magnetoresistance to the resistance of the sample; $\Delta R(B)$ linearly increases with increasing B .

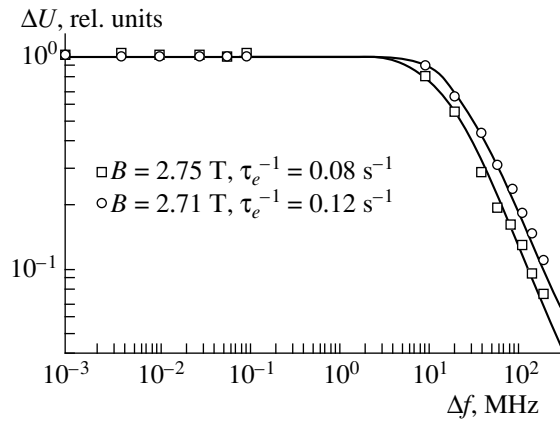


Fig. 2. Dependence of the signal magnitude on the modulation frequency for two close values of magnetic field: $B = 2.75$ and 2.71 T. For low frequencies Δf , the values of ΔU are normalized to the photoconductivity signal at a frequency of 1 kHz.

$5 \times 10^{11} \text{ cm}^{-2}$ and the mobility $\mu = 2 \times 10^5 \text{ cm}^2/\text{Vs}$ at $T = 4.2 \text{ K}$. As in our previous experiments [4], for the direct measurements of the energy relaxation time, we used the mm-wave spectroscopy with high temporal resolution.

The specific feature of the case under study is that in magnetic field the energy relaxation time varies over wide limits, from 10^{-9} to 10^{-7} s. To measure small relaxation times $\tau_e < 10^{-8}$ s, we used a mm-wave spectrometer in which the electromagnetic radiation was incident on the sample from two backward-wave tube oscillators shifted in frequency by Δf . The absorption of electromagnetic radiation by free carriers or bonded carriers in the region of localized states leads to a variation in the sample resistance ΔR and the appearance of a photoconductivity signal ΔU at the frequency Δf . The

relaxation time of the mm-wave photoconductivity signal is equal to the energy relaxation time of the carriers in the absence of the bolometric effect, and it is determined by the frequency dependence of the quantity ΔU :

$$\Delta U(\Delta f) = \frac{\Delta U(\Delta f = 0)}{\sqrt{1 + (2\pi\Delta f\tau_e)^2}}.$$

The frequency stability of the backward-wave tube oscillators allows one to perform such measurements at frequencies $\Delta f > 10^7 \text{ Hz}$ ($\tau_e < 10^{-8}$ s). To measure large relaxation times, the electromagnetic radiation of a backward-wave tube oscillator is modulated by supplying a modulating voltage at the frequency Δf to the anode circuit of the tube.

The measurements of τ_e in quasi-equilibrium conditions impose stringent requirements on the sensitivity of the measuring equipment because of the weak dependence of the resistance of the structure R on the electron temperature. The sensitivity of the equipment used in our experiments allowed us to perform the measurements with the minimum electromagnetic radiation power incident on the sample and the dc power $P_{e \text{ min}} \approx 5 \times 10^{-17}$ watt per electron, which corresponds to an increase in the temperature of free two-dimensional carriers by $\Delta T_e \approx 0.1\text{--}0.3 \text{ K}$; this value is quite suitable for the measurements at the temperature $T = 4.2 \text{ K}$.

3. The measurements of the nonresonant mm-wave photoconductivity ΔU showed that, in a magnetic field, the quantity ΔU exhibits oscillations similar to the Shubnikov–de Haas oscillations of the resistance (Fig. 1). The measured values of ΔU shown in the figure correspond to the low-frequency modulation of the mm-wave radiation ($\Delta f = 2 \text{ kHz}$). The signal is a bipolar one: in the vicinity of the resistance minimum in the Shubnikov–de Haas oscillations, ΔU corresponds to the growth of resistance with the absorption of electromagnetic radiation, and in the vicinity of the maximum in the resistance R it corresponds to a decrease in the resistance. The first maximum observed in the signal at $B \approx 0.4 \text{ T}$ corresponds to the cyclotron resonance at the frequency of the mm-wave radiation. The signal ΔU is asymmetric about zero: it is considerably greater at the minimum in the resistance R . The bipolarity of the signal is related to different mechanisms of photoconductivity (the electron gas heating near the resistance maximum and the hopping mechanism at the resistance minimum), and it was also observed in other experiments (e.g., [11]).

The photoconductivity signal ΔU was measured as a function of the frequency Δf in magnetic fields from 0 to 3.6 T. As an illustration, in Fig. 2 we present the dependences of the photoconductivity signal ΔU on Δf for two close values of B ($B_1 = 2.75 \text{ T}$ and $B_2 = 2.71 \text{ T}$) corresponding to the vicinity of the minimum in R . One can see that the frequency dependences noticeably differ from each other. From the measurements of $\Delta U(\Delta f)$,

we obtained the values of $\tau_e^{-1}(B)$ (Fig. 3). The absence of the experimental values of τ_e^{-1} for $B = 2.9\text{--}3.3$ and $2.3\text{--}2.5$ T is related to the insufficient sensitivity of the experimental setup at high frequencies $\Delta f > 10^6$ Hz (in these intervals of magnetic fields B , the photoconductivity signal is too weak; see Fig. 1).

The experiment shows that, with increasing B , the electron–phonon interaction becomes less efficient (τ_e^{-1} decreases), and, at $B \approx 1.2$ T, the energy relaxation rate decreases by an order of magnitude relative to its value at $B = 0$. In the quantum Hall effect regime ($B > 1$ T, the filling factor $\nu = \epsilon_F/\hbar\omega_C < 8$), the dependence $\tau_e^{-1}(B)$ exhibits oscillations. The depth of these oscillations increases with increasing B . In Fig. 3, the arrows indicate the values of B corresponding to the maximum photoconductivity signal (the minimum R). One can see that, for $B > 2.5$ T, the quantity τ_e^{-1} is minimum in magnetic fields B corresponding to the resistance minimum, while, for $B < 2$ T, the minimum τ_e^{-1} corresponds to the resistance maximum.

4. We begin the analysis of our experimental results with some estimates. The measurements are performed at $T = 4.2$ K. The prevailing component of the electron–phonon interaction is the scattering due to the deformation potential; the wave vector of a thermal phonon $q = kT/\hbar S$ is of the order of the wave vector of a two-dimensional electron at the Fermi surface k_F ($kT/\hbar S \approx k_F$). In the absence of magnetic field, the wave vectors of the phonons that take part in the electron–phonon interaction are limited in the direction perpendicular to the 2D layer by the transverse dimension of the layer a_0 : $q_\perp < 1/a_0$, and, in the layer plane, according to the conservation laws, we obtain the limitation $q_\parallel < 2k_F$. Thus, all phonon states fill a cylinder of height $1/a_0 \approx 10^6$ cm $^{-1}$ for typical GaAs/AlGaAs 2D structures and of radius q_\parallel (for the concentration of two-dimensional carriers $n_S \approx 5 \times 10^{11}$ cm $^{-2}$, we obtain $q_\parallel \approx 4 \times 10^6$ cm $^{-1} \approx 1/a$). In a magnetic field, only the radius of the cylinder is changed; namely, q_\parallel is limited by the magnetic length $l_B = \sqrt{\hbar/eB}$: $q_\parallel < 1/l_B$ ($1/l_B = 3.9 \times 10^5$ T $^{-0.5}$ cm $^{-1}$). For magnetic fields $B < 4$ T, we have $q_{\parallel B \neq 0} \ll q_{\parallel B = 0}$. These estimates show that, in the absence of magnetic field, the energy relaxation rate is determined by the emission of phonons with the energy $\approx kT$, while, in magnetic field, such phonons can be emitted only at low angles to the magnetic field direction, which considerably reduces the electron energy relaxation rate. Hence, the substantial decrease in τ_e^{-1} observed in the experiment in magnetic field can be attributed to the change in the spectrum of phonons involved in the electron–phonon interaction.

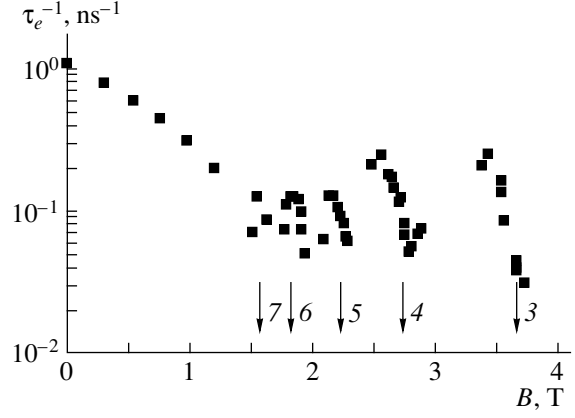


Fig. 3. Dependence of the inverse relaxation time of the photoconductivity signal τ_e^{-1} on the magnetic field B . The arrows indicate the values of B at which R takes its minimum values. The numbers near the arrows show the values of the filling factor ν corresponding to the given magnetic fields.

In a major part of the magnetic field range, the values of τ_e^{-1} obtained from our experiments describe the inelastic relaxation related to the electron transitions within the Landau levels. In fact, the energy of the mm-wave radiation quantum is $\hbar\omega = 0.6$ meV. For the maximum value of B , we obtain the estimate $\hbar\omega_C \approx 6$ meV; then, for magnetic fields $B > 1$ T, we have $\hbar\omega \gg \hbar\omega_C$. In the experiment, the temperature was $T = 4.2$ K, and $kT \approx 0.4$ meV. Since $kT \ll \hbar\omega_C$, in this magnetic field range the electrons occupy only the Landau levels with the energy $\epsilon \leq \epsilon_F$. Therefore, the absorption of a radiation quantum with the energy $\hbar\omega \ll \hbar\omega_C$ can be accompanied only by the electron transitions within the last occupied Landau level. These transitions lead either to the carrier heating when ϵ_F is coincident with the energy of the Landau level in the region of delocalized states, or to nonresonant hopping between localized states when ϵ_F falls between the Landau levels in the region of localized states. In this case, the energy relaxation of excited carriers may occur only at the expense of the electron transitions within the Landau level. According to Kent *et al.* [9], the energy relaxation rate for the intralevel relaxation strongly depends on the density of states; i.e., the energy relaxation rate is maximum when the Fermi level coincides with the Landau level, and it is minimum when ϵ_F falls in the region of localized states. Only in low magnetic fields, in the transient region of B where $kT < \hbar\omega_C$, interlevel transitions are possible owing to the presence of several partially filled Landau levels. As a result of the absorption of electromagnetic radiation, the heated carriers may emit phonons of both low energies $\epsilon_{\text{ph}} \ll \hbar\omega_C$ and high energies $\epsilon_{\text{ph}} \approx \hbar\omega_C$ (the interlevel ones). Although the probability of the emission of high-energy phonons is much less than that of the low-energy phonons, the

former make a substantial contribution to the relaxation because of the large change in the electron energy in every event of emission. The energy relaxation rate for to these transitions is maximum when the Fermi level is in the region of localized states between the Landau levels [9]. In this case, the probability of the emission of phonons with the energy $\epsilon_{\text{ph}} \ll \hbar\omega_C$ is increased, since, for $kT < \hbar\omega_C$, the delocalized states at the Landau level with the energy $\epsilon > \epsilon_F$ are filled to a greater extent, and the delocalized states at the Landau level with the energy $\epsilon < \epsilon_F$ are filled to a lesser extent, as compared to the case of the Fermi level lying in the region of delocalized states.

The conditions corresponding to the energy relaxation at the expense of the intralevel transitions are fully realized in our experiment for $B > 2$ T: the quantity τ_e^{-1} exhibits two deep minima at the magnetic fields corresponding to the minima in the resistance R ($\nu = 3, 4$). At $B = 3.6$ T, the value of τ_e^{-1} is an order of magnitude less than that corresponding to the maximum in R . Evidently, the depth of the oscillations should grow with increasing B (at lower filling factors ν) and with decreasing T . The oscillations of the quantity τ_e^{-1} are also observed for intermediate magnetic fields $1 \text{ T} < B < 2 \text{ T}$. However, at the values of B corresponding to the minimum resistance R , a maximum in τ_e^{-1} is observed, which presumably testifies to the substantial contribution of the interlevel electron–phonon transitions to the energy relaxation of two-dimensional electrons. In this interval of magnetic fields B , the depth of the oscillations is much less than at low values of ν .

Thus, we measured the energy relaxation times of 2D electrons in quasi-equilibrium conditions, in magnetic fields corresponding to the quantum Hall effect regime. We have shown that the quantization of the electron energy in magnetic field leads to a sharp decrease in the energy relaxation rate and to oscillations of the energy relaxation time that are similar to the

Shubnikov–de Haas oscillations. Under weakly non-equilibrium conditions, the energy relaxation in high magnetic fields is determined by the electron–phonon transitions within the Landau level. The contribution of the electron–phonon transitions between the Landau levels manifests itself in intermediate magnetic fields.

This work was supported by the Russian Foundation for Basic Research (grant no. 98-02-897), the Program of the State Support of Leading Scientific Schools (project no. 96-02-96426), the Program “Physics of Solid Nanostructures,” and the grant “Universities of Russia.”

REFERENCES

1. B. K. Ridley, Rep. Progr. Phys. **54**, 169 (1991).
2. V. Karpus, Fiz. Tekh. Poluprovodn. **22**, 439 (1988).
3. H. Sakaki, K. Hirakawa, J. Yoshino, *et al.*, Surf. Sci. **142**, 306 (1994); K. Hirakawa and H. Sakaki, Appl. Phys. Lett. **49**, 889 (1986).
4. A. A. Verevkin, N. G. Ptitsina, G. M. Chulkova, *et al.*, Phys. Rev. B **53**, R7592 (1996); A. A. Verevkin, N. G. Ptitsina, G. M. Chulkova, *et al.*, Pis'ma Zh. Éksp. Teor. Fiz. **61**, 579 (1995) [JETP Lett. **61**, 591 (1995)].
5. H. A. J. M. Reinen, T. T. J. M. Berendschot, R. J. H. Kap-pert, *et al.*, Solid State Commun. **65**, 1495 (1988).
6. G. A. Toombs, F. W. Sheard, D. Neilson, *et al.*, Solid State Commun. **64**, 577 (1987).
7. F. Dietzel, W. Dietsche, and K. Ploog, Phys. Rev. B **48**, 4713 (1993).
8. K. Benedict, J. Phys. Condens. Matter **4**, 4083 (1992).
9. A. J. Kent, R. E. Strickland, K. R. Spickland, *et al.*, Phys. Rev. B **54**, 2019 (1996).
10. B. R. A. Neves, N. Mori, P. H. Beton, *et al.*, Phys. Rev. B **52**, 4666 (1995).
11. N. M. Grodnenskiĭ, K. V. Starostin, and D. V. Galchenkov, Pis'ma Zh. Éksp. Teor. Fiz. **43**, 54 (1986) [JETP Lett. **43**, 70 (1986)].

Translated by E. Golyamina

CONDENSED
MATTER

Magnetic and Magneto-optical Properties of Fe/Pt and Fe/Pt/Fe Thin-Film Magnetic Structures

E. E. Shalygina¹, N. I. Tsidaeva, and M. A. Karsanova

Physics Department, Moscow State University, Moscow, 119899 Russia

Received November 16, 1999

Abstract—Results of a study of magnetic and magneto-optical properties of Fe/Pt double-layer and Fe/Pt/Fe three-layer thin-film magnetic structures are presented. A strong effect of the Pt layer on magnetic properties of the studied samples was revealed. It was established that the saturation field of three-layer magnetic structures has an oscillating magnitude with varying Pt layer thickness, and the oscillation period is a function of the Fe layer thickness. The data obtained are explained by the presence of exchange interaction between the Fe layers via the Pt layer. A strong effect of Pt on spectral dependences of the equatorial Kerr effect in the thin-film structures under study is revealed. © 2000 MAIK “Nauka/Interperiodica”.

PACS numbers: 75.70.Cn, 75.70.Ak, 78.20.Ls

In recent years, a great number of experimental and theoretical works were devoted to the investigation of magnetic anisotropy, remagnetization processes, and kinetic and magneto-optical properties of thin-film magnetic structures (TFMS). This is determined by the fact that a number of new phenomena such as giant magnetoresistance [1], oscillating exchange interaction between ferromagnetic layers via a nonmagnetic layer [2], and quantum dimensional effects [3] were revealed in these samples at the end of 1980s and at the beginning of 1990s. The results of previous studies were found to be very useful in solving several problems in magnetic phenomena physics. In particular, significant information was obtained concerning the influence of the interface between a magnetic film and a substrate (as well as between magnetic and nonmagnetic layers) on the formation of kinetic, magnetic, and magneto-optical properties of TFMS. However, studying the effect of the thickness and composition of magnetic and nonmagnetic layers on these properties of TFMS still deserves attention. Note that the results of these studies are of practical importance, because they can be used for the development of new thin-film systems for modern spin microelectronics. It is obvious that, for the correct solution of this problem, the first step should be a study of double-layer and three-layer samples with alternating magnetic and nonmagnetic layers.

The objective of this investigation was to study the influence of the thickness of magnetic and nonmagnetic layers on the magnetic and magneto-optical properties of Fe/Pt and Fe/Pt/Fe thin-film structures.

The samples under study were obtained with the magnetron sputtering technique. After the adhesion at the temperature $T = 150^\circ\text{C}$, the basic pressure in the

vacuum chamber was 10^{-9} Torr. Argon was the working gas. Its pressure was $\sim 10^{-4}$ Torr. The magnetic layer thickness t_{Fe} in double-layer structures was varied from 2 to 100 nm, and the thickness t_{Pt} of the nonmagnetic layer deposited between the magnetic film and substrate was 0–20 nm. In three-layer structures, t_{Fe} and t_{Pt} were varied from 2.5 to 10 nm and from 0.4 to 4 nm, respectively. Samples were coated with a 10-nm carbon layer in order to avoid oxidation. Structural features of the samples under study were investigated with an X-ray diffractometer. The data of X-ray diffraction scattering showed the presence of pronounced interfaces between magnetic and nonmagnetic layers.

The magnetic characteristics (hysteresis loops, saturation fields, coercive force) of the studied samples were measured on a magneto-optical magnetometer by using the equatorial Kerr effect (EKE) δ . Here, $\delta = (I - I_0)/I_0$, where I and I_0 are the intensities of the light reflected from the magnetized and nonmagnetized samples, respectively. An external magnetic field was applied in the sample plane perpendicular to the light incidence plane. The magneto-optical properties of the TFMS under study were investigated on a magneto-optical setup based on a DMP-4 double monochromator. Dispersion dependences of the EKE were measured in an energy range of the incident light quanta of $1.5 < \hbar\omega < 4.2$ eV. The angle of light incidence on the sample was 65° . A detailed description of the facilities is presented in [4, 5]. All measurements were performed at room temperature in air.

The data obtained in measurements of magnetic characteristics indicated that all the samples under study are characterized by planar magnetic anisotropy (the easy magnetization axis lies in their plane). The hysteresis loops along the easy magnetization axis for double-layer samples had an almost rectangular shape.

¹ e-mail: shal@magn.phys.msu.u

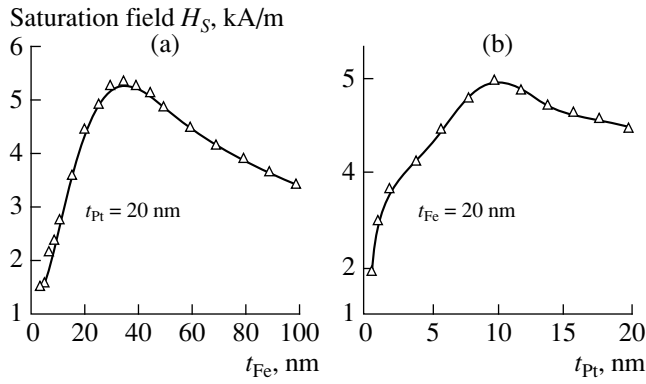


Fig. 1. Saturation field H_S of Fe/Pt double-layer samples as a function of the thickness of (a) a Fe film and (b) a Pt layer deposited between the film and substrate at fixed thicknesses of nonmagnetic and magnetic layers, respectively. The energy of the incident light quanta is constant ($\hbar\omega = 2.0$ eV).

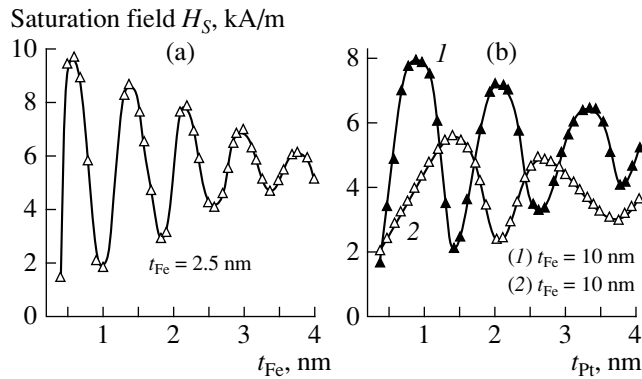


Fig. 2. Saturation field H_S of Fe/Pt/Fe three-layer samples as a function of the Pt layer thickness: (a) $t_{Fe} = 2.5$ nm; and (b) $t_{Fe} = 5$ and 10 nm (curves 1 and 2, respectively).

The ratio to the residual magnetization to the saturation magnetization (M_R/M_S) was 0.95–0.98. The M_R/M_S value increased with a decrease in the Fe layer thickness.

Figure 1 shows the saturation field H_S of the double-layer samples under study as a function of the (a) Fe film and (b) Pt layer thicknesses t_{Fe} and t_{Pt} at fixed t_{Pt} and t_{Fe} , respectively. Figure 2 shows typical dependences of the saturation field H_S on the nonmagnetic layer thickness at fixed t_{Fe} for Fe/Pt/Fe structures. As we see in Fig. 1a, at fixed t_{Pt} , H_S rises with t_{Fe} increasing up to 35 nm, and then decreases when t_{Fe} changes from 40 to 100 nm. At a fixed Fe layer thickness, the saturation field H_S has a maximum at $t_{Pt} \approx 10$ nm (b). Note that the behavior of the coercive force H_S as a function of t_{Fe} and t_{Pt} of double-layer samples coincides with the functions $H_S(t_{Fe})$ and $H_S(t_{Pt})$. The results obtained can be explained by using data of the structural analysis of

samples. X-ray diffraction studies have shown that the double-layer samples have a polycrystalline structure with a predominant $\{111\}$ texture parallel to the sample surface. It was established that the degree to which samples are textured depends on both the Fe film and Pt layer thicknesses. It is known [6] that the samples textured to a higher degree are characterized by a higher saturation field and coercive force. We observed precisely such a relationship between the magnetic and structural properties of the studied Fe/Pt double-layer samples.

Figure 2 shows that the saturation field of Fe/Pt/Fe samples oscillates as a function of t_{Pt} , and the oscillation period Λ depends on t_{Fe} . In particular, Λ is 0.8, 1.2, and 2 nm at $t_{Fe} = 2.5, 5,$ and 10 nm, respectively. As the thicknesses of both Fe films and Pt separating layer increase, the saturation field of the samples under study decreases. The data obtained can be explained by the existence of exchange interaction between ferromagnetic layers via the nonmagnetic layer and by its oscillatory behavior with changing thickness of the nonmagnetic layer [7, 8]. Rather high experimental Λ values show that this parameter should be estimated theoretically taking into account the quantum dimensional effect [3]; i.e., changes in the electron structure of an ultrathin layer (the appearance of so-called quantum well states) as compared to a bulk material should be taken into consideration. As shown in [8], in this case, Λ differs from π/κ_F (κ_F is the Fermi wave vector), which is ~ 0.3 nm for most of metals. The photoelectron emission technique is a direct method for observing quantum well states in ultrathin films. Unfortunately, as far as we know, photoemission studies of Pt layers on magnetic and nonmagnetic substrates were not performed. As a result, we could not compare the obtained Λ values with data of other studies. As to changes in Λ with increasing magnetic layer thickness, the following facts can be mentioned. Calculations performed in recent years [9] have shown that Λ must increase with increasing magnetic layer thickness. In fact, we observed experimentally such a change in Λ . A decrease in H_S with increasing t_{Fe} and t_{Pt} is determined by the weakening of the exchange interaction between magnetic layers.

Figure 3 shows dispersion dependences of the EKE of (a) Fe/Pt double-layer and (b) Fe/Pt/Fe three-layer samples with $t_{Fe} = 2.5$ nm and various thicknesses of the Pt layer. Figure 4 shows dispersion dependences of the EKE of Fe/Pt double-layer samples with $t_{Fe} = 5$ nm (a) and 10 nm (b) with $t_{Pt} = 0$ and 2 nm. As we see in Fig. 3, the peak of $\delta(\hbar\omega)$ in an energy range of the incident quanta of 1.8–1.9 eV, which is typical of the spectral dependence of the EKE for bulk iron, decreases with increasing t_{Pt} , and a new peak appears in the UV. These spectra are modified as compared to bulk iron. This can be explained by the effect of Pt on magneto-optical properties of the thin-film structures under study. Neutron diffraction studies show [10] that Pt may have a

magnetic moment of $\sim 0.3 - 0.4\mu_B$ in alloys with, for example, Co. The spin-orbital energy of the Pt $5d$ -states is fairly high. As a result, the electron wave functions of the Fe $3d$ - and Pt $5d$ -states overlap at the interface of adjacent Fe and Pt layers. This electron interface effect ($3d$ - $5d$ hybridization) determines the exchange-induced spin polarization of platinum, thus resulting in a significant contribution of Pt to the nondiagonal component of the permittivity tensor of the sample under study. This results in a strong modification of the dispersion dependences of the EKE in Fe/Pt and Fe/Pt/Fe structures in comparison with bulk Fe. According to the data [11], the strongest effect of Pt on magneto-optical properties of multilayer thin film structures and alloys with Pt must be manifested in the near UV region. This is confirmed by our results. Note that the presence of spin-polarized Pt actually determines oscillatory dependences of the saturation field and coercive force of three-layer samples with changing t_{Pt} .

The electron interface effect described above must obviously depend on the thicknesses of both the Fe and Pt layers. The following fact should also be taken into consideration. It is known [12] that a magneto-optical signal (in particular, related to the EKE) may depend on the sample thickness t , if $t < t_{inf}$, where t_{inf} is the information depth of the magneto-optical signal (i.e., the depth at which the magneto-optical signal forms). In [13], it was shown experimentally that $t_{inf} = 15-20$ nm for Fe for incident light quanta with energies of $1.5 < \hbar < 4.2$ eV. The total thickness of the double- and three-layer samples studied by us was smaller than t_{inf} . Thus, at equal Fe layer thicknesses, the EKE in three-layer structures must exceed that in double-layer structures (approximately, by a factor of two). The data in Fig. 3 confirm this inference. The quantitative comparison of the EKE values for double- and three-layer samples shows that the influence of the Pt layer on the EKE in the second case is stronger than in the first one; i.e., the presence of two Fe/Pt interfaces in three-layer structures should be taken into consideration.

The comparison of the data obtained for double-layer structures (Figs. 3a and 4) shows that the values of $\delta_{Fe}(t_{Pt} = 0) - \delta_{Fe/Pt}(t_{Pt} = 2 \text{ nm})$ are virtually the same for $t_{Fe} = 2.5, 5, \text{ and } 10$ nm, while the EKE magnitudes increase with increasing thickness of the Fe film. Similar results were obtained for samples with another Pt layer thickness. However, we see in Figs. 3 and 4 that the Pt layer effect on the EKE is enhanced with the growth of its thickness. It was established that this enhancement holds up to $t_{Pt} \approx 4$ nm.

Hence, magnetic and magneto-optical properties of Fe/Pt and Fe/Pt/Fe thin film structures were studied. An oscillatory dependence of the saturation field H_S of three-layer structures on the Pt layer thickness was revealed. The period of H_S oscillations was determined to be dependent on the Fe film thickness. The data obtained were explained by the presence of exchange

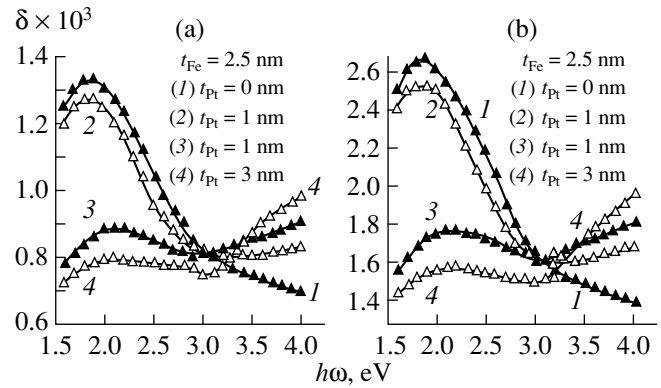


Fig. 3. Dispersion dependences of the EKE for (a) Fe/Pt and (b) Fe/Pt/Fe thin film structures at fixed thicknesses of the Fe layer and various Pt layer thicknesses.

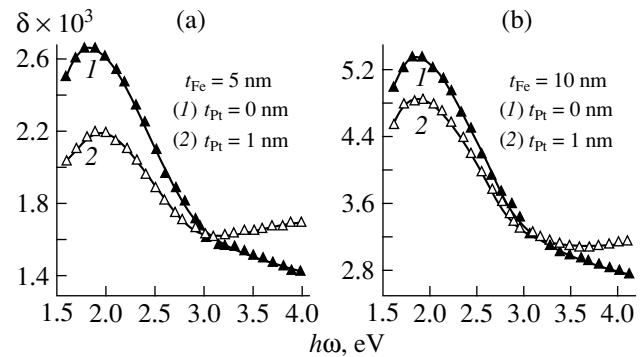


Fig. 4. Dispersion dependences of the EKE for Fe/Pt double-layer samples with (a) $t_{Fe} = 5$ nm and (b) $t_{Fe} = 10$ nm; $t_{Pt} = 0$ and 2 nm.

interaction between ferromagnetic layers via a non-magnetic layer in three-layer systems.

A strong effect of the Pt layer on dispersion dependences of the EKE in Fe/Pt and Fe/Pt/Fe thin film structures was revealed. This fact was explained by the exchange-induced ($3d$ - $5d$ hybridization) spin polarization of Pt. It was established that the modification of EKE spectra of the studied samples is enhanced with increasing thickness of the Pt layer up to $t_{Pt} \approx 4$ nm, and the influence of Pt in three-layer samples is approximately twice as strong as in double-layer structures.

This work was supported in part by the Russian Foundation for Basic Research, project no. 99-02-16595.

REFERENCES

1. M. N. Baibich, J. M. Broto, A. Fert, *et al.*, Phys. Rev. Lett. **61**, 2472 (1988).
2. S. S. P. Parkin, N. More, and K. P. Roche, Phys. Rev. Lett. **64**, 2304 (1990).
3. J. E. Ortega, F. J. Himpsel, G. J. Mankey, *et al.*, Phys. Rev. B: Condens. Matter **47**, 1540 (1993).

4. G. S. Krinchik, E. E. Chepurova, B. N. Ponomarev, *et al.*, Fiz. Tverd. Tela (St. Petersburg) **28**, 2862 (1986).
5. G. S. Krinchik, E. E. Chepurova, and Sh. V. Egamov, Zh. Éksp. Teor. Fiz. **74**, 714 (1978) [Sov. Phys. JETP **47**, 375 (1978)].
6. C. J. Lin, G. L. Gorman, C. H. Lee, *et al.*, J. Magn. Magn. Mater. **93**, 194 (1991).
7. S. P. Parkin, R. Bhadra, and K. P. Roche, Phys. Rev. Lett. **66**, 2152 (1991).
8. P. Bruno, Phys. Rev. B: Condens. Matter. **52**, 411 (1995).
9. L. Nordstrom, P. Lang, R. Zeller, *et al.*, Phys. Rev. B: Condens. Matter **50**, 13058 (1994).
10. K. H. J. Buschow, P. G. van Engen, and R. Jongebreur, J. Magn. Magn. Mater. **38**, 1 (1983).
11. D. Weller, W. Reim, and K. Spröl, J. Magn. Magn. Mater. **93**, 183 (1991).
12. G. Traeger, L. Wensel, and A. Hubert, Phys. Status Solidi A **131**, 201 (1992).
13. E. E. Shalygina, L. V. Kozlovskii, and Du Syan'bo, Vestn. Mosk. Univ., Ser. 3 **36**, 51 (1995).

Translated by A. Seferov

CONDENSED
MATTER

Superfluid Molecular Hydrogen

V. S. Vorob'ev¹ and S. P. Malysenko

IVTAN (Institute of High Temperatures) Scientific Association, Russian Academy of Sciences, Moscow, 127412 Russia

Received October 20, 1999; in final form, December 8, 1999

Abstract—In order to produce a supercooled liquid phase of molecular hydrogen that may possibly change at a sufficiently low temperature to a superfluid state, it is suggested to reduce the temperature of its equilibrium coexistence with the solid phase by means of developing different pressures in these phases through the use of linear mechanical pressure on the solid phase or of external electric field. The thermodynamic functions of hydrogen are calculated in both the stable and metastable regions; its phase diagram and the region of possible transition to a superfluid state are also found. The values of excess pressure on the solid phase and of external electric field intensity are estimated, which are necessary for the stabilization of this state. © 2000 MAIK “Nauka/Interperiodica”.

PACS numbers: 05.70.Fh, 05.70.Ce, 05.30.Ip, 67.40.Kh

Ginzburg and Sobyenin [1] predicted that liquid hydrogen supercooled to a sufficiently high degree relative to its normal freezing point might transform to a superfluid state. In order to reach such states, they suggested in [1] to use negative pressures causing a decrease of the melting point. This could not be accomplished experimentally because of the low cavitation strength of liquid hydrogen [2]. In so doing, it is still not quite clear whether this is due to hard-to-eliminate external effects or to the fundamental impossibility of a higher degree of extension of liquid because of reaching the parameters of the line of loss of thermodynamic stability of a uniformly extended liquid relative to the gas phase (spinodal). In recent years, a rebirth of interest in this problem is observed [3, 4]; however, even today, both the relative position of the spinodal (of the liquid–solid melting line and of the line of possible λ -transition on the phase diagram) and the possible ways of attaining these states remain unclear.

We used the method of [5] to calculate the thermodynamic functions of hydrogen. The indeterminate functions contained in this method were found from the condition of agreement between the thermodynamic functions calculated by this method and the thermodynamic functions of hydrogen given in the reference book [6] and taking into account all of the presently available experimental data. The thus-calculated isotherms of pressure for the liquid state are in good agreement with the experimental data, and the accuracy of this method is quite sufficient for finding the thermodynamic functions at low temperatures for both the stable and metastable states.

The phase diagram for hydrogen is given in Fig. 1. In this diagram, the melting curve is continued into the region of negative pressures and temperatures lying

below the triple point temperature. Fine lines indicate the family of isochors of liquid hydrogen in the regions of stable and metastable states. It is well known that the envelope of this family gives the boundary of absolute stability of the liquid state with respect to the gas state, i.e., liquid-gas spinodal. Such a spinodal is evident in Fig. 1; one can see that it limits the possibility of extending the melting curve into the negative pressure region by values of the order of $p \approx -90$ atm. A line corresponding to a possible transition of liquid hydrogen to a superfluid state may be plotted in this diagram. For this purpose, we will use the recent data on the temperature of λ -transition T_λ of Bose's liquid, obtained by Apenko [7], with the effective diameter of the molecule equal to 2.7 Å [8]. The respective line is plotted on the P – T plane (line 5). One can see that this line divides the states corresponding to supercooled liquid in the P – T plane into normal and superfluid regions at a transition temperature of 1–2 K. Note the existence of a positive pressure region, in which supercooled liquid hydrogen may become superfluid. At the same time, it is fundamentally impossible to attain the λ -transition by moving along the melting curve in the negative pressure region, because melting curve 4 continued into the negative pressure region reaches the spinodal before reaching the intersection with the line of λ -transition.

The dependence of the chemical potentials of phases on pressure at constant temperature is given in Fig. 2 for the temperature $T = 13.8$ K (triple point temperature) and $T = 1$ K. Lines 1 in this and subsequent figures indicate the solid phase, with lines 2 indicating the liquid phase and lines 3, the gas phase. One can see that, in the case of $T = 13.8$ K, all three lines intersect at a single point at a low positive pressure corresponding to the experimentally obtained value of pressure at the triple point $p_T = 0.07$ atm. In the case of $T = 1$ K, the chemical potential of the liquid phase in the entire

¹ e-mail: vrvb@mail.ru

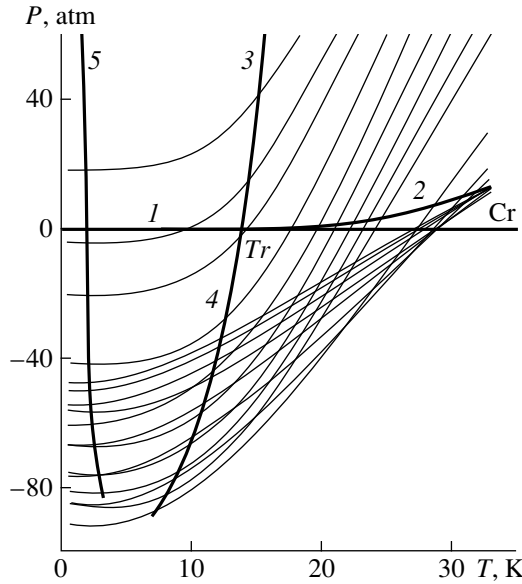


Fig. 1. The P - T diagram for hydrogen. Bold lines: (1) sublimation curve, (2) evaporation curve, (3) melting curve, (4) melting curve continued into the metastable region, (5) boundary of the superconductivity region ($d = 2.7 \text{ \AA}$); T_r , triple point; Cr , critical point. Fine lines: family of isochors for the values of v varying from 12.5 (uppermost isochor) to 31 cm^3/g (lowermost isochor). The envelope of these isochors forms the spinodal.

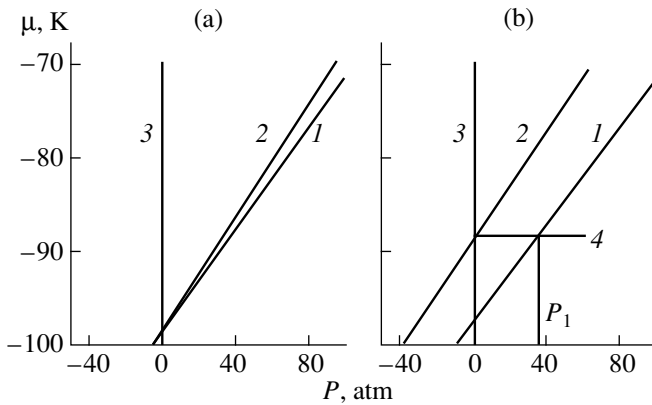


Fig. 2. The chemical potentials for the solid phase (line 1), liquid phase (line 2), and gas phase (line 3) as functions of pressure: (a) at $T = 13.8 \text{ K}$, (b) at $T = 1 \text{ K}$. Line 4 in (b) gives the value of chemical potential for different pressures of the phases.

range of its existence is higher than that of the solid phase, and the point of intersection of isotherms is absent.

In order to attain the λ -transition in liquid hydrogen, we suggest to make use of the fact that, in the case of phase equilibria under conditions of unequal pressures in the phases, one of the phases may stably exist with the parameters corresponding to those of metastable

states in the absence of external effects. In particular, if excess pressure is somehow developed on the solid phase, its equilibrium coexistence is possible with supercooled liquid at lower pressures.

We will estimate the excess pressure to be exerted on the solid phase of hydrogen at $T \approx 1 \text{ K}$ for the latter phase to find itself in equilibrium with the supercooled liquid phase at pressures which rule out the possible formation of the gas phase. For the liquid phase, this is actually accomplished at very low positive pressures $p > p_r$. We find in Fig. 2b that the pressure difference must be about 30 atm. In this case, a liquid which is superfluid may coexist in equilibrium with the solid phase. Without discussing the concrete methods of developing additional mechanical pressure on the solid phase, we will just note that a serious obstacle in the way may be provided by the low mechanical strength of solid hydrogen. According to the data of [9], Young's modulus and the elongation corresponding to the ultimate strength at this temperature are equal to 3300 atm and 0.08, respectively. Hence, it follows that solid hydrogen is capable of withstanding, without changing its form, a pressure of the order of 26 atm. Within the accuracy of our calculations, this value coincides with that of required excess pressure.

Another way of developing different pressures in the phases is by exposing a two-phase system to the effect of external electric field [10]. We will define the conditions in which, because of the presence of external field, hydrogen will not crystallize at temperatures corresponding to the λ -transition. We will treat a two-phase system of (1) a solid and (2) a liquid at constant temperature in an external electric field. The condition of phase equilibrium may be written as

$$\begin{aligned} \mu_1(p_1) - \frac{E_1^2}{8\pi} \left(\frac{\partial \epsilon_1}{\partial \rho_1} \right)_T \pm \frac{\epsilon_1 E_1^2 - \epsilon_2 E_2^2}{8\pi \rho_1} \\ = \mu_2(p_2) - \frac{E_2^2}{8\pi} \left(\frac{\partial \epsilon_2}{\partial \rho_2} \right)_T, \end{aligned} \quad (1)$$

where $\mu_1(p_1)$ and $\mu_2(p_2)$ are the chemical potentials of the material of the phases at pressures p_1 and p_2 , E is the electric field intensity, and ϵ is the dielectric constant. The plus sign indicates the case when the field is generated by constant charges; the minus sign, the case when the field is generated by constant potentials. We expand $\mu_2(p_2)$ in (1) in series at the point $p_2 = p_1$ and take into account that the chemical potential of the condensed phase is in fact proportional to pressure to derive

$$\begin{aligned} \mu_2(p_1) \approx \mu_1(p_1) + \frac{p_1 - p_2}{8\pi \rho_1 \rho_2} \\ \times \left[E_1^2 \left(\rho_1 \left(\frac{\partial \epsilon_1}{\partial \rho_1} \right)_T \mp \epsilon_1 \right) \pm \epsilon_2 E_2^2 \right], \end{aligned} \quad (2)$$

where p_0 is the pressure corresponding to the phase equilibrium in the absence of field.

We will once again turn to Fig. 2b. We wish to obtain the liquid state in the presence of a field in the pressure region left of the curve of the pressure dependence of chemical potential (curve 3), that is, at $p_1 > p_g \approx 0$. We assume the Clausius-Mosotti relation is valid, as well as that the field is generated by constant potentials and the phase boundary is parallel to the lines of intensity, to derive from (2) the intensity of electric field supporting the existence of the liquid phase at small positive pressures,

$$E = \sqrt{\frac{-24\pi(\mu_1(0) - \mu_2(0))\rho_1\rho_2}{(\epsilon_1^2 + 4\epsilon_1 - 2 - 3\epsilon_2)(\rho_1 - \rho_2)}}. \quad (3)$$

For hydrogen, the values borrowed from [6] are $\epsilon_1 = 1.3$, $\epsilon_2 = 1.25$, $\rho_1 = 0.087 \text{ g/cm}^3$, and $\rho_2 = 0.078 \text{ g/cm}^3$. The value of the difference of the chemical potentials of the phases at $T = 1 \text{ K}$ and $p = 0$, taken from the graph of Fig. 2b, is -10 K . We substitute all of these values into (3) to obtain the value of $E = 4 \times 10^7 \text{ V/cm}$. In so doing, hydrogen will remain liquid and may transform to a superfluid state. However, this value of intensity may exceed those of intensity of dielectric breakdown. No direct data are available on the electric strength of hydrogen under these conditions. According to the data of Gerhold [11], the values of intensity of breakdown at a normal temperature of boiling in liquid helium do not exceed $1 \times 10^6 \text{ V/cm}$; in liquid nitrogen, $1 \times 10^7 \text{ V/cm}$. These values are lower than required for our purposes. However, a decrease in temperature may cause an increase in the intensity of breakdown. The latter may also be increased by using pulse voltage [11].

If a system is subjected to mechanical stimulation, an instability of the compressed crystal-liquid interface may be observed. As is shown theoretically in [12], the effect of indefinitely small nonhydrostatic components of the field of stresses inside an elastic crystal may cause the transformation of indifferent equilibrium into unstable one. We assume the surface tension of solid hydrogen to be $\sigma \cong 5 \text{ dyn/cm}$ and the velocity of longitudinal and transverse sound waves to be 2.2×10^5 and $1.2 \times 10^5 \text{ cm/s}$, respectively [9], to derive the value of the critical wavelength estimated by formula of [12] of the order of $0.2 \text{ }\mu\text{m}$. The instability may lead to the system transition to a disperse state. In order to overcome this instability, a certain complication of the method of compression of solid hydrogen is required, for example, exerting one-sided pressure on the solid phase with the aid of a porous piston with the pore size of less than

the critical wavelength. For superfluid hydrogen, this piston will be absolutely permeable. The question of whether a similar instability arises under electrostatic stimulation still remains unclear.

Note further that, in the case of both mechanical and field compression of crystal, the intensity of external effect on the liquid-solid two-phase system, which is required to attain the parameters of expected λ -transition in liquid hydrogen, proves to be close to the limits of its mechanical or electric strength, and the possibility of practical realization of the suggested methods depends on how surmountable are the difficulties involved.

We are grateful to V.L. Ginzburg, A.A. Sobyenin, and S.M. Apenko for bringing this problem to our attention.

This study received support from the Russian Foundation for Basic Research (grants 99-02-16596 and 99-02-16619).

REFERENCES

1. V. L. Ginzburg and A. A. Sobyenin, *Pis'ma Zh. Éksp. Teor. Fiz.* **15**, 343 (1972) [*JETP Lett.* **15**, 242 (1972)].
2. V. A. Aculichev and V. A. Bulanov, *Sov. Phys. JETP* **38**, 329 (1974); *Sov. Phys. Acoust.* **20**, 107 (1974); *Sov. Phys. Acoust.* **20**, 501 (1975).
3. H. J. Maris, G. M. Seidel, and T. E. Huber, *J. Low Temp. Phys.* **51**, 471 (1983).
4. M. C. Cordillo and D. M. Ceperley, *Phys. Rev. Lett.* **79**, 3010 (1997).
5. V. S. Vorob'ev, *Pis'ma Zh. Éksp. Teor. Fiz.* **62**, 557 (1995) [*JETP Lett.* **62**, 574 (1995)]; *Zh. Éksp. Teor. Fiz.* **109**, 161 (1996) [*JETP* **82**, 85 (1996)].
6. McCarty, *Hydrogen Technological Survey—Thermophysical Properties* (NASA, Washington, 1975).
7. S. M. Apenko, *Phys. Rev. B* **60**, 3052 (1999).
8. J. Wilks, *The Properties of Liquid and Solid Helium* (Clarendon, Oxford, 1967).
9. *The Properties of Condensed Phases of Hydrogen and Oxygen*, Ed. by B. I. Verkin (Naukova Dumka, Kiev, 1984).
10. V. S. Vorob'ev and S. P. Malysenko, *Phys. Rev. E* **56**, 3959 (1997).
11. J. Gerhold, in *Proceedings of 13th International Conference on Dielectric Liquids (ICDL'99)*, Naras, Japan, 1999, pp. 365, 445.
12. M. A. Grinfel'd, *Dokl. Akad. Nauk SSSR* **290**, 1358 (1986) [*Sov. Phys. Doklady* **31**, 831 (1986)].

Translated by H. Bronstein

Inertial Parameters and Superfluid-to-Normal Phase Transition in Superdeformed Bands¹

I. M. Pavlichenkov²

Russian Research Center Kurchatov Institute, Moscow, 123182 Russia

Received December 1, 1999

Abstract—The quasiclassically exact solution for the second inertial parameter \mathcal{B} is found in a self-consistent way. It is shown that superdeformation and nonuniform pairing arising from the rotation-induced pair density significantly reduce this parameter. The new signature for the transition from pairing to normal phase is suggested in terms of the variation \mathcal{B}/\mathcal{A} versus spin. Experimental data indicate the existence of such a transition in the three SD mass regions. © 2000 MAIK “Nauka/Interperiodica”.

PACS numbers: 21.10.Gv, 21.10.Re, 21.60.Fw, 23.20.Lv, 27.60.+j

One of the amazing features of superdeformed (SD) rotational bands is the extreme regularity of their rotational spectra: an SD nucleus is the best quantum rotor known in nature. In spite of the fact that numerous theoretical calculations successfully reproduce the measured intraband γ -ray energies (see, e.g., [1, 2]), the underlying microscopic mechanism of this phenomenon is still not understood well. To explain this regularity, we use in the present paper the parameterization of its rotational energy by the two-term formula

$$E(I) = \mathcal{A}I(I+1) + \mathcal{B}I^2(I+1)^2, \quad (1)$$

which is valid for an axially symmetric deformed nucleus with $K = 0$. The inertial parameters $\mathcal{A} = \hbar^2/2\mathfrak{S}^{(1)}$ ($\mathfrak{S}^{(1)}$ is the kinematic moment of inertia) and \mathcal{B} are the objects of our investigation. The coefficient \mathcal{B} characterizes the nonadiabatic properties of a band and is very sensitive to its internal structure. The ratio \mathcal{B}/\mathcal{A} determines the convergence radius [3] of the two-parameter formula (1), which is of the order of 100 for the bands in the 80 and 150 mass regions, and 40 in the 130 and 190 ones. Faster convergence is obtained with the Harris formula,

$$E(\omega) = E_0 + \frac{1}{2}\alpha\omega^2 + \frac{3}{4}\beta\omega^4, \quad (2)$$

which is based on the fourth-order cranking expansion

$$\alpha = \frac{1}{\omega} \text{Sp}(l_x \rho^{(1)}), \quad \beta = \frac{1}{\omega^3} \text{Sp}(l_x \rho^{(3)}), \quad (3)$$

where $\rho^{(n)}$ is the n th correction to the nucleus density matrix, l_x is the single-particle orbital angular momentum projection on the rotational axis x perpendicular to

the symmetry axis z , and ω is the rotational frequency. For simplicity, we will deal with the parameter β .

The problem of the microscopic calculation of the parameter \mathcal{B} for normal deformed (ND) nuclei has attracted considerable attention. This value is formed mainly by four effects: vibration–rotation interaction, centrifugal stretching, perturbation of the quasiparticle motion, and attenuation of pair correlation by the Coriolis force (Mottelson–Valatin effect). The last two are dominant for well-deformed nuclei, as has already been shown in the first attempts at obtaining \mathcal{B} [4, 5]. Unfortunately, the results of these and many other works cannot be used for the superdeformation. The formulas of [5] have been obtained in the limit of the monopole pairing interaction (the uniform pairing), which is not adequate at SD shapes as shown in [6]. In the more sophisticated work [4], the gauge invariant pairing interaction allows one to study the effect of nonuniform pairing. However, this approach is also limited because it neglects the coupling between major shells (the limit of close transitions in Migdal’s terminology [7]). Thus, despite a number of publications on the subject, the correct cranking self-consistent solution for the \mathcal{B} coefficient has not been found.

We used the quasiclassical method of [4] to derive the following expression for the β parameter in the superfluid phase:

$$\beta_s = -\frac{\hbar^4}{4\Delta^2} \sum l_{12}^x l_{23}^x l_{34}^x l_{41}^x \times F(x_{12}, x_{23}, x_{34}, x_{41}) \delta(\epsilon_1 - \epsilon_F), \quad (4)$$

where the summation indices $i = 1, 2, 3, 4$ refer to the single-particle states i in the nonrotating mean field with the energy ϵ_i . The δ -function means that the summation over the states 1 is restricted by a small interval at the Fermi energy ϵ_F [7]. The dimensionless values

¹ This article was submitted by the author in English.

² e-mail: pavi@cerber.polyn.kiae.su

$x_{i\bar{i}} = (\varepsilon_i - \varepsilon_{\bar{i}})/2\Delta$, where Δ is the state-independent pairing gap at $\omega = 0$, correspond to energy differences between states permitted by the selection rules for the matrix element of l_x . The function F depending on these values may be written as follows:

$$F = \sum_{k=0}^3 \hat{P}_k G_{12} + \sum_{k=0}^1 \hat{P}_k H_{13} - 8D_2^2 x_{12} x_{23} x_{34} x_{41} h(x_{13}), \quad (5)$$

where

$$\begin{aligned} G_{12} = & \frac{g(x_{12})}{x_{23} x_{41} x_{13} x_{24}} \{ (1 - D_1 x_{12}^2) [-1 - x_{12}^2 - x_{23} x_{41}] \\ & + D_1 [x_{23}^2 (1 - x_{12} x_{24}) + x_{41}^2 (1 + x_{12} x_{13})] \\ & + D_1^2 x_{23} x_{34} x_{41} (x_{23} + x_{41}) + D_1^3 x_{12} x_{23}^2 x_{34} x_{41}^2] \\ & + D_1 (x_{34} - D_1 x_{12} x_{23} x_{41}) \\ & \times (x_{34} + x_{12} x_{13} x_{24} - D_1 x_{12} x_{23} x_{41}) \}, \\ H_{13} = & \frac{h(x_{13})}{x_{12} x_{23} x_{34} x_{41}} (1 - D_1 (x_{12}^2 + x_{23}^2 + x_{34}^2 + x_{41}^2)^2 \\ & + D_1^2 (x_{12} x_{41} + x_{23} x_{34})], \end{aligned} \quad (6)$$

and

$$h(x) = (1 + x^2)g(x), \quad g(x) = \frac{\text{argsh}x}{x\sqrt{1+x^2}}. \quad (7)$$

Here, \hat{P}_k are permutation operators in the space of four indices $i, i \bmod 4 = \bar{i}$: $\hat{P}_k x_{i, \bar{i}} = x_{i+k, \bar{i}+k}$.

Equation (4) multiplied by ω^3 is the third-order cranking correction to the total angular momentum of the neutron or proton system. Its derivation will be described in a forthcoming paper. We now want to emphasize that (4) represents the first theoretically correct expression for the high-order effect of the Coriolis-pairing interaction at fixed deformation. The result is obtained by taking into account the effect of rotation on the Cooper pairs in the gauge invariant form. This effect is described by the first, $\Delta^{(1)}(\mathbf{r}) = -i\hbar^2 \omega D_1 \hat{l}_x / 2\Delta$, and the second, $\Delta^{(2)}(\mathbf{r}) = \hbar^4 \omega^2 D_2 \hat{l}_x^2 / 4\Delta^3$, corrections to the pairing energy. The amplitudes D_1 and D_2 of the nonuniform pairing fields are found in a self-consistent way. The coordinate dependent pairing field is crucial for conservation of a nucleon current. The theory incorporating the nonuniform pairing allows one also to consider the different limiting cases for the inertial parameters, which make possible the study of an interplay between rapid rotation, pairing correlations, and mean field deformation in an SD band.

In order to consider this problem quantitatively, we will use the axially deformed oscillator potential with

the frequencies ω_x and ω_z on the corresponding axes. In this model, the matrix element l_{12}^x is nonzero for the two types of transitions: (i) transitions inside a single oscillator shell, for which $x_{12} = \pm v_1$; (ii) transitions over a shell with $x_{12} = \pm v_2$. The quantities v_1 and v_2 are the well-known parameters involved in the moment of inertia [7]:

$$v_{1,2} = \frac{\hbar(\omega_x \mp \omega_z)}{2\Delta} = \frac{k \mp 1}{2\xi k^{2/3}}, \quad \xi = \frac{\Delta}{\hbar\omega_0}, \quad (8)$$

where $\hbar\omega_0 = 41A^{-1/3}$ MeV. Here and below we use the axis or frequency ratio $k = c/a = \omega_x/\omega_z$ and the volume conservation condition $\omega_x^2 \omega_z = \omega_0^3$. Both the values v_1 and v_2 are large for the superdeformation. The final expression for the parameter β_s in the oscillator potential is

$$\beta_s = \beta_0 \Phi(\xi, k) = \frac{AM^3(k+1)^4}{1875\hbar^2 k^{4/3}} R^6 \Phi(\xi, k), \quad (9)$$

where $R = 1.2A^{1/3}$ fm is the radius of the sphere, the volume of which is equal to that of the spheroid with the half-axes $a < c$, M is the nucleon mass, and A is the number of nucleons. The function Φ , along with its limiting cases, is shown in Fig. 1. It is seen that nonuniform pairing substantially reduces the parameter β_s in agreement with the estimation of [6]. On the other hand, the contribution of distant transitions is minor for small ξ . Nevertheless, the latter are necessary to obtain the hydrodynamic limit (see below). Since $\Phi \sim 1$ for a reasonable pairing gap, $\Delta \sim 0.5$ MeV, the order of the value β_s is $\hbar^4(A/\varepsilon_F)^3$. This, along with the estimation $\mathcal{A} \sim \varepsilon_F A^{-5/3}$, gives $\mathcal{B}/\mathcal{A} \sim A^{-2}$, which overestimates the minimal value of this ratio in all the SD mass regions.

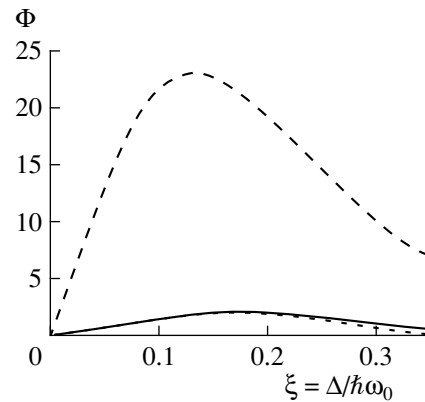


Fig. 1. Plot of the function Φ from (9) against the dimensionless value ξ , for the axis ratio $c/a = 2$. The solid, dotted, and dashed lines correspond respectively to the exact value, the limit of close transitions, and the uniform pairing. The scale on the abscissa should be multiplied by a factor of approximately 7.7 for nuclei in the $A \sim 150$ mass region to obtain a gap energy in MeV.

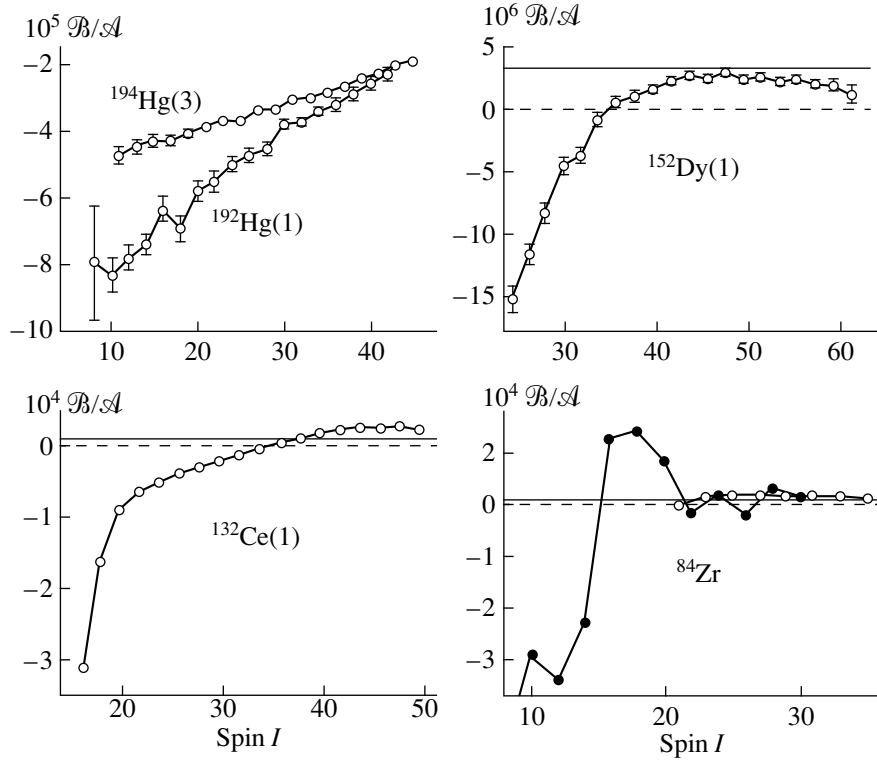


Fig. 2. \mathcal{B}/\mathcal{A} ratio versus spin for the SD (open circles) and ND (full circles) bands with mainly collective behavior. The solid straight line is the limiting value (11) with the deformation c/a found from the quadrupole moment. Error bars (if they are greater than symbols) include γ -ray energy uncertainties only.

Thus, a small Δ and nonuniform pairing do not solve the problem of the SD band regularity.

Let us consider first the limiting case $\Delta = 0$. The correct expression for the β parameter in the normal phase has the form

$$\beta_n = -\hbar^4 \sum_{l_{12}^x l_{23}^x l_{34}^x l_{41}^x} \sum_{k=0}^3 \hat{P}_k \left\{ \frac{n_1}{\varepsilon_{12} \varepsilon_{13} \varepsilon_{14}} \right\}. \quad (10)$$

The odd function of the differences $\varepsilon_{ir} = \varepsilon_i - \varepsilon_r$ leads to the cancellation of the main terms in sum (10) that substantially decreases the value of β_n , $\beta_n \sim \hbar^4 A^{7/3} / \varepsilon_F^3$. Note that the centrifugal stretching effect has the same order $\beta_{str} \sim \beta_n$. Its contribution is small compared to that of β_s , but it should not be overlooked for an unpaired system. For the oscillator potential, we have the following expression for a nucleus consisting of z protons and N neutrons:

$$\frac{\mathcal{B}_n}{\mathcal{A}_n} = -2.56 \frac{(k^4 - 10k^2 + 1)k^{2/3}}{(k^2 + 1)^3 A^{8/3}} \times \left[\left(\frac{2Z}{A} \right)^{1/3} + \left(\frac{2N}{A} \right)^{1/3} \right]. \quad (11)$$

It is seen that this value is positive for the prolate nuclei with $c/a < 3.15$, whereas \mathcal{B}_s is always negative. Thus,

with an increase of the spin I , the ratio \mathcal{B}/\mathcal{A} has to change sign and to approach its limiting value $\mathcal{B}_n/\mathcal{A}_n \sim A^{-8/3}$ ($\sim 10^{-6}$ for the SD bands in the 80 and 150 mass region).

One can therefore conclude that there are two distinct regions in the variation of \mathcal{B}/\mathcal{A} versus I . The lower part of an SD band is characterized by a gradual decrease of the pairing gap Δ . According to (9), the ratio \mathcal{B}/\mathcal{A} should exhibit a sharp increase. Then it changes sign and approaches the plateau (11) at the top of a band because the deformation c/a depends weakly on spin in both the superdeformed and normal phase. Such behavior of the \mathcal{B}/\mathcal{A} ratio is the signature of the pairing phase transition.

We have analyzed all the SD bands of [8] with known or suggested spins of levels. Figure 2 shows the variation of the \mathcal{B}/\mathcal{A} ratio with I obtained for bands with different internal structure and different rotational frequencies. Apart from the bands $^{192}\text{Hg}(1)$ and $^{194}\text{Hg}(3)$, where frequencies are so low that \mathcal{B}/\mathcal{A} rises continuously in the superfluid phase, and $^{84}\text{Zr}(1)$, the pairing for which is quenched completely and \mathcal{B}/\mathcal{A} is close to the limiting value (11), all other bands display the behavior described above. It is important to note that such behavior is observed for the ND yrast band of ^{84}Zr , where \mathcal{B}/\mathcal{A} reaches the same limiting value (11)

as in the SD band $^{84}\text{Zr}(1)$. There are other ND yrast bands of ^{168}Yb and ^{168}Hf with the pair phase transition, the experimental evidence of which has been discussed previously in terms of the canonical variables [9] and the spectrum of single-particle states [9, 10]. These bands exhibit the same features. Thus, the plots of Fig. 2 demonstrate the universality of the superfluid-to-normal phase transition for SD and ND bands.

The next limit we want to consider is that of a large pairing gap Δ . In this case, the nonuniform pairing is essential and the leading terms in the function Φ are those proportional to the powers of D_1 and D_2^2 . They result in the limiting expression $\Phi \sim (\hbar\omega_0/\Delta)^2$. Thus, for the very strong pairing ($\Delta \gg \hbar\omega_0$), when the size of the Cooper pair $R\hbar\omega_0/\Delta$ becomes much less than the nuclear radius, the parameter \mathcal{B}_s vanishes in agreement with the hydrodynamic equations of the ideal liquid [3]. In the limit of an extremely large deformation, $c/a \rightarrow \infty$, a needle-shaped nucleus with pairing correlations rotates as a rigid body, $\mathfrak{S} = \mathfrak{S}_{\text{rig}}$, $\mathcal{B}_s = 0$. For the finite but large deformation, the deviations from these values are proportional to $(a/c)^{4/3}$. This means that all nucleons with the exclusion of a small sphere in the center of a nucleus are completely involved in rotational motion. Finally, for small deformations we have $\mathcal{B}_s \sim (c/a - 1)^{-6}$, which is comparable to the vibration-rotation interaction [4].

Unlike the limiting value (11), it is impossible to compare the ratio $\mathcal{B}_s/\mathcal{A}_s$ with experiment because the proton (Δ_π) and neutron (Δ_ν) pairing gaps are unknown for the SD bands. In such a case, we try to solve the inverse problem. The equations for the two inertial parameters

$$\begin{aligned} \alpha\mathcal{A}/\mathfrak{S}_{\text{rig}} &= Z\varphi(\xi_\pi, k) + N\varphi(\xi_\nu, k), \\ \beta\mathcal{A}/\beta_0 &= Z\Phi(\xi_\pi, k) + N\Phi(\xi_\nu, k), \end{aligned} \quad (12)$$

allow, in principle, to find ξ_π and ξ_ν if we use the quadrupole moment for extraction of the axis ratio k . Unfortunately, this system does not have a solution

because the oscillator potential overestimates the moment of inertia and, to a greater extent, the β parameter. A more realistic potential should be used to solve this problem.

In summary, the exact solution for the inertial parameter \mathcal{B} in the superfluid phase allows one to show that neither superdeformation nor nonuniform pairing arising from rotation-induced pair density are responsible for the extreme regularity of the SD rotational spectra. The regularity of the SD bands in the 80 and 150 mass regions is explained by the transition from the superfluid to normal phase. The new signature of this transition is manifested in the characteristic dependence of the ratio \mathcal{B}/\mathcal{A} with the spin I . Application of this criterion to experimental data indicates the existence of the phase transition in the SD bands of the three mass regions.

This work was supported in part by the Russian Foundation for Basic Research (grant no. 96-02-16115).

REFERENCES

1. W. Satula and R. Wyss, Phys. Rev. C **50**, 2888 (1994).
2. Yang-Sun, Jing-ye Zhang, and M. Guidry, Phys. Rev. Lett. **78**, 2321 (1997).
3. A. Bohr and B. R. Mottelson, *Nuclear Structure* (Benjamin, New York, 1975), Vol. II.
4. Yu. T. Grin' and I. M. Pavlichenkov, Sov. Phys. JETP **16**, 333 (1963); I. M. Pavlichenkov, Nucl. Phys. **55**, 225 (1964).
5. E. R. Marshalek, Phys. Rev. **139**, B770 (1965); *ibid.* **158**, 993 (1967).
6. I. Hamamoto and W. Nazarewicz, Phys. Rev. C **49**, 2489 (1994).
7. A. B. Migdal, Nucl. Phys. **13**, 655 (1959).
8. B. Singh and B. Firestone, Nucl. Data Sheets **78**, 1 (1996).
9. J. D. Garrett, G. B. Hagemann, and B. Herskind, Ann. Rev. Nucl. Part. Sci. **36**, 419 (1986).
10. J. R. B. Oliveira, S. Frauendorf, M. A. Deleplanque *et al.*, Phys. Rev. C **47**, R926 (1993).

Cooperative Nonradiative Cross-Relaxation in Crystals of $\text{La}_{1-x}\text{Ce}_x\text{F}_3$ Solid Solutions

T. T. Basiev¹, M. E. Doroshenko, and V. V. Osiko

Institute of General Physics, Russian Academy of Sciences, Moscow, 117942 Russia

Received December 7, 1999

Abstract—The phenomenon of concentration quenching of the luminescence from donor ions in crystals of $\text{La}_{1-x}\text{Ce}_x\text{F}_3$ solid solutions was studied. A cooperative nonradiative energy transfer from a single excited neodymium ion to a cooperative acceptor representing a couple of cerium ions, as well as from a single erbium ion to three cerium atoms (also forming a cooperative acceptor center), was observed. © 2000 MAIK “Nauka/Interperiodica”.

PACS: 32.50.+d, 42.62.Fi, 42.65.-k

INTRODUCTION

As is known, the traditional mechanism of nonradiative energy transfer between two particles—energy donor and acceptor—is operative only in the case of resonance between electron or electron-vibrational transitions, which corresponds to a nonzero value of the overlap integral between the donor emission and acceptor absorption spectra [1]. This mechanism results in a linear relationship between the acceptor concentration and the rate of luminescence quenching in the initial and kinetic stages [2, 3]. Until now, a single type of the cooperative nonradiative energy transfer, called the cooperative sensitization, was known in the physics of activated crystals. According to this, the nonradiative energy transfer takes place simultaneously from two (or more) ions, representing a cooperative donor, to a single acceptor ion possessing a higher transition energy [4–6].

In this work, we have observed and studied the cooperative energy transfer of a new type (called the cooperative quenching or cross-relaxation), in which the nonradiative energy is transferred from a single ion (donor) simultaneously to two (or more) ions representing a cooperative acceptor. According to this mechanism, the electron excitation energy initially localized on a single donor ion is instantaneously shared between two (or more) acceptor ions, whereby the excitation is multiplied and delocalized in space. The concentration dependence of the rate of this nonradiative energy transfer in the kinetic stage becomes significantly nonlinear, obeying a quadratic law for the twinned cooperative acceptor and a cubic law, for the triple cooperative acceptor.

We have studied crystals of the $\text{La}_{1-x}\text{Ce}_x\text{F}_3$ solid solution system with the content of Ce^{3+} ions varied from 0 to 100% ($x = 0-1$). The crystals were coacti-

vated by doping with a small concentration of trivalent ions of neodymium or erbium. A special feature of the electron structure of cerium is the absence of any electron levels and optical transitions in a broad range of energies and frequencies ($3500-30000\text{ cm}^{-1}$). This circumstance prevents cerium ions from acting as traditional acceptors or sensitizers in the process of energy transfer in the visible and near-IR spectral range. The only optical transition in the $4f$ electron shell of Ce^{3+} is the ${}^2F_{5/2}-{}^2F_{7/2}$ transition at a frequency of $1500-3000\text{ cm}^{-1}$ falling within the middle IR spectral range. In contrast, neodymium and erbium ions exhibit a broad spectrum of luminescent transitions, including both close to and far from resonance with the ${}^2F_{5/2}-{}^2F_{7/2}$ transition in cerium ions. At the same time, Ce^{3+} ions possess physicochemical properties that are very close to those of lanthanum ions (La^{3+}) and may substitute for up to 100% of the latter ions without any significant distortion of the crystal lattice and without modification of the optical properties of the activator ions.

EXPERIMENTAL RESULTS

The crystals of $\text{La}_{1-x}\text{Ce}_x\text{F}_3 : \text{Nd}$ and $\text{La}_{1-x}\text{Ce}_x\text{F}_3 : \text{Er}$ were grown by the Bridgman technology in graphite crucibles under fluorine-containing atmosphere. The activator concentration was 0.3 at % for Nd^{3+} ions and 1 at % for Er^{3+} ions. The Nd^{3+} and Er^{3+} donors were excited by second harmonic of a Q-modulated GGG : Nd^{3+} laser or by nanosecond radiation pulses of a tunable sapphire-titanium laser. The donor luminescence was dispersed by a grating monochromator and detected using a multiplier phototube ($0.8-1\text{ }\mu\text{m}$ wavelength range) or a germanium photodiode ($1.5-1.6\text{ }\mu\text{m}$). The decay kinetics of luminescence from Nd^{3+} and Er^{3+} ions was measured in a real time mode, with the signal accumulation and discrimination against noise per-

¹ e-mail: basiev@lst.gpi.ru

formed with aid of a TDS-380 two-channel digital oscillograph linked to a personal computer.

Figure 1 shows diagrams of the energy levels of Nd^{3+} , Er^{3+} , and Ce^{3+} ions in LaF_3 crystals. The schemes of energy levels and the spectra of transitions in $\text{La}_{1-x}\text{Ce}_x\text{F}_3$ crystals remain virtually unchanged upon variation of the parameter x , which is explained by close proximity of the ionic radii of La^{3+} and Ce^{3+} as well as of the crystal lattice parameters of LaF_3 and CeF_3 . A comparison of energies of the absorption transition in cerium ion and the luminescent transitions in erbium and neodymium ions shows that only a four-micron transition ${}^4S_{3/2}\text{--}{}^4F_{9/2}$ in erbium exhibits a good resonance with the ${}^2F_{5/2}\text{--}{}^2F_{7/2}$ transition in cerium, which is necessary for a nonradiative donor–acceptor energy transfer by the traditional mechanism. There are no resonances with absorption in cerium ion for the ${}^4I_{13/2}\text{--}{}^4I_{15/2}$ ($\lambda = 1.5\text{--}1.6\ \mu\text{m}$) transition in erbium ion and the ${}^4F_{3/2}\text{--}{}^4I_{15/2}$ ($\lambda = 0.89\text{--}1.8\ \mu\text{m}$) transition in neodymium ion. Another important circumstance is a “short” phonon spectrum of LaF_3 and CeF_3 crystals, which does not extend beyond $400\ \text{cm}^{-1}$. This may provide for a good resonance in the interaction and optical excitation energy transfer from a single Nd^{3+} ion ($h\nu_{\text{fl}} = 5500\ \text{cm}^{-1}$) simultaneously to two Ce^{3+} ions ($2h\nu_{\text{abs}} = 4000\text{--}6000\ \text{cm}^{-1}$) and from a single Er^{3+} ion ($h\nu_{\text{fl}} = 7000\ \text{cm}^{-1}$) simultaneously to three Ce^{3+} ions ($3h\nu_{\text{abs}} = 6200\text{--}8400\ \text{cm}^{-1}$).

At the first stage of this work, we have measured the decay kinetics of luminescence from the ${}^4S_{3/2}$ level of Er^{3+} ion in $\text{La}_{1-x}\text{Ce}_x\text{F}_3$ crystals where the traditional donor–acceptor energy transfer from erbium to cerium ion is possible. Figure 2a shows a plot of the lifetime $\tau({}^4S_{3/2})$ of erbium ions in the initial (ordered) decay stage versus their concentration. Figure 2b presents the corresponding values of the luminescence quenching rate $W_{\text{Er} \rightarrow \text{Ce}}(x) = 1/\tau(x) - 1/\tau(0)$ in the ordered (kinetic) stage versus the cerium ion concentration. As seen from this figure, the observed variation of the quenching rate is quite well approximated by a straight line, in agreement with the linear concentration dependence anticipated for the kinetic limit or the ordered direct energy transfer: $W^m = aW^0x$, where a is the coordination number of the cationic sublattice and W^0 is the rate of elementary quenching reaction for a pair of ions at a minimum possible distance R_{min} [2]. As seen from Fig. 2b, the maximum quenching rate for pure cerium fluoride (CeF_3) obtained by summation over the whole cerium sublattice (with all the lattice sites adjacent to the donor ion being occupied by acceptors) has proved to be $W_{\text{Er} \rightarrow \text{Ce}}^m(100\%) = 2.7 \times 10^5\ \text{s}^{-1}$. This value is of the same order of magnitude as the rate of the direct self-quenching process $\text{Nd} \rightarrow \text{Nd}$ in a NdF_3 crystal and in

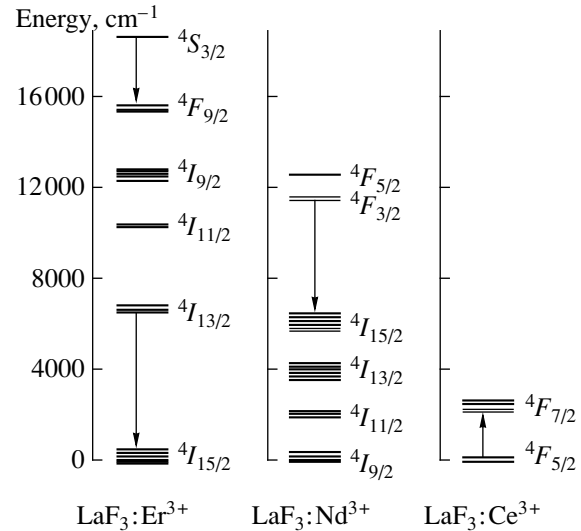


Fig. 1. Energy level diagram for Nd^{3+} , Er^{3+} , and Ce^{3+} ions in LaF_3 crystals.

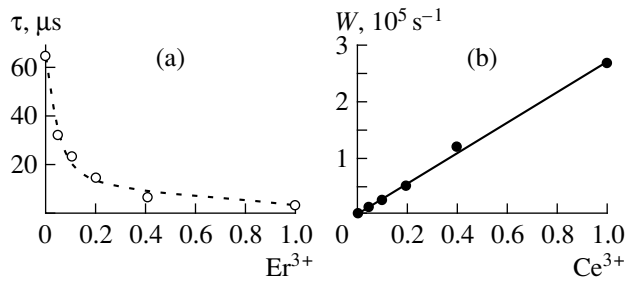


Fig. 2. The plots of (a) lifetime of the ${}^4S_{3/2}$ level of Er^{3+} ions versus their concentration and (b) energy transfer rate $W_{\text{Er} \rightarrow \text{Ce}}$ versus Ce^{3+} ion concentration in crystals of $\text{La}_{1-x}\text{Ce}_x\text{F}_3$ solid solutions: (circles) experimental points; (solid line) linear approximation.

a crystal with 100% acceptor concentration, the latter value being $W_{\text{Nd} \rightarrow \text{Nd}}^m(100\%) = 0.72 \times 10^5\ \text{s}^{-1}$ [7].

Within the framework of the model of generalized coordination spheres proposed and justified in [8], we may separate 12 nearest neighbor acceptors ($a = 12$, the first generalized coordination sphere) in the nearest environment of an impurity ion in the NdF_3 lattice. These acceptors occur at a minimum distance from the donor, $R_{\text{min}} = 4.15 \pm 0.15\ \text{\AA}$. Estimates [8] show that contribution of the first coordination sphere (i.e., of the interaction with nearest neighbors) to the total relaxation rate is dominating even if the multipole donor–acceptor interaction is governed by the longest-range mechanism—the dipole–dipole interaction ($W \sim R_{\text{DA}}^{-6}$). In this case, upon replacing the sum over all cationic lattice sites of the cerium sublattice by the sum over

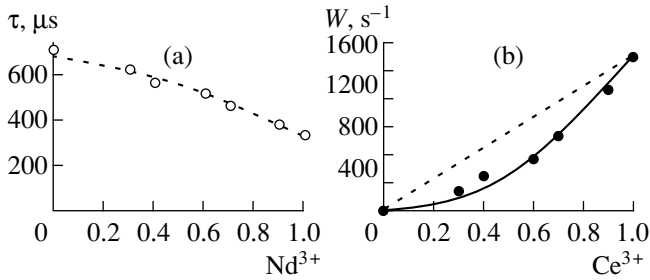


Fig. 3. The plots of (a) lifetime of the metastable $^4F_{3/2}$ level of Nd^{3+} ions versus their concentration and (b) cooperative energy transfer rate $W_{\text{Nd}-2\text{Ce}}$ versus Ce^{3+} ion concentration in crystals of $\text{La}_{1-x}\text{Ce}_x\text{F}_3$ solid solutions: (circles) experimental points; (dashed line) linear approximation; (solid line) quadratic approximation.

12 nearest neighbor cerium ions in the first coordination shell of the donor, we may estimate the rate of the elementary quenching interaction in the ion pair $\text{Er} \rightarrow \text{Ce}$ or $\text{Nd} \rightarrow \text{Nd}$ at a minimum possible donor-acceptor distance: $W_{\text{Er} \rightarrow \text{Ce}}^0 \approx 270000/12 = 22500 \text{ s}^{-1}$, $W_{\text{Nd} \rightarrow \text{Nd}} \approx 72000/12 = 6000 \text{ s}^{-1}$.

COOPERATIVE QUENCHING OF THE LUMINESCENCE OF NEODYMIUM AND ERBIUM IONS IN CRYSTALS OF $\text{La}_{1-x}\text{Ce}_x\text{F}_3$ SOLID SOLUTIONS

The luminescence decay kinetics measured for the metastable level $^4F_{3/2}$ of the Nd^{3+} ion in $\text{La}_{1-x}\text{Ce}_x\text{F}_3$ solid solution crystals exhibited a single-exponent character. Figure 3a (open circles) shows the lifetime of this level as function of the concentration of neodymium ions. As seen, the lifetime exhibits a monotonic decrease with increasing concentration which, provided a constant rate of the radiative decay, is evidence of the increasing rate of the concentration luminescence quenching. Figure 3b (black circles) presents the corresponding values of the rate of nonradiative energy transfer calculated by the formula $W_{\text{Nd} \rightarrow 2\text{Ce}}(x) = 1/\tau(x) - 1/\tau(0)$ using the measured $\tau(x)$ values, where $\tau(0)$ is the radiative lifetime of the given metastable level. Constancy of the $\tau(0)$ value and the radiative transition probabilities for Nd^{3+} ion in the whole series of $\text{La}_{1-x}\text{Ce}_x\text{F}_3$ solid solutions was checked by measured optical absorption spectra of neodymium and by the results of calculations according to the Judd–Ofelt theory. The solid curve in Fig. 3b shows approximation of the experimental data by the quenching rate plotted as a quadratic function of the concentration of cerium ion, and the dashed line represents the linear quenching law. As seen from this figure, the experiment reveals a significantly nonlinear (close to quadratic) variation of the quenching rate $W_{\text{Nd} \rightarrow 2\text{Ce}}$ with the Ce^{3+} ion concentration up to 100% (pure CeF_3). This behavior differs from

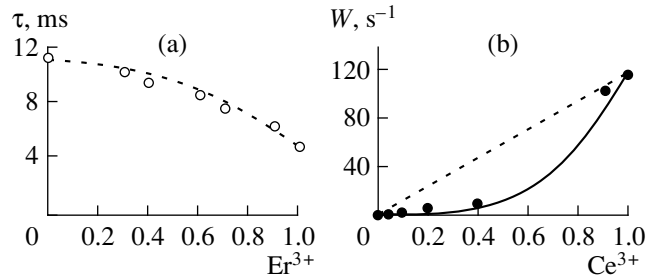


Fig. 4. The plots of (a) lifetime of the $^4I_{13/2}$ level of Er^{3+} ions versus their concentration and (b) energy transfer rate $W_{\text{Er}-3\text{Ce}}$ versus Ce^{3+} ion concentration in crystals of $\text{La}_{1-x}\text{Ce}_x\text{F}_3$ solid solutions: (circles) experimental points; (dashed line) linear approximation; (solid line) cubic approximation.

that corresponding to the traditional mechanism of concentration quenching described by the linear law, observed, for example, for the direct energy transfer $\text{Er} \rightarrow \text{Ce}$ or $\text{Nd} \rightarrow \text{Nd}$ in highly concentrated solid solutions of the $\text{La}_{1-x}\text{Ce}_x\text{F}_3 : \text{Er}$ and $\text{La}_{1-x}\text{Ce}_x\text{F}_3$ systems.

In a random uncorrelated process of substituting Ce^{3+} ions for La^{3+} in the LaF_3 lattice, a single cooperative acceptor of the Ce_2 type is formed when two cerium ions simultaneously fall within the first (nearest-neighbor) coordinate sphere of a donor ion (Nd^{3+} or Er^{3+}). According to the probability theory, the probability of this event is proportional to the product of the corresponding probabilities for single Ce^{3+} ions and, hence, to the square of the concentration of Ce^{3+} ions in the $\text{La}_{1-x}\text{Ce}_x\text{F}_3$ solid solution. The probability of formation of a triple cooperative acceptor (Ce_3) corresponds to still more pronounced deviation from linearity and is proportional to (at least) cubic concentration of Ce^{3+} ions. From this, we may conclude that sharp nonlinearity of the concentration dependence of the quenching rate at sufficiently large concentration of cerium ions (when these ions are arranged in an ordered manner, that is, at a minimum distance) around a donor ion (Nd^{3+} or Er^{3+}) is experimental evidence of the fact that the cooperative quenching mechanism is operative.

The total rate of the cooperative quenching in pure cerium fluoride (CeF_3) was $W_{\text{Nd} \rightarrow 2\text{Ce}}^m(100\%) = 1570 \text{ s}^{-1}$, which is markedly (tens to hundreds times) lower compared to the value for the traditional linear mechanism of energy transfer $\text{Er} \rightarrow \text{Ce}$ or $\text{Nd} \rightarrow \text{Nd}$ (see above). Considering pairs (Ce_2) as independent cooperative acceptors situated in the first (nearest neighbor) coordination sphere of a donor (neodymium ion) and assuming their coordination number in CeF_3 to be $12/2 = 6$, we may estimate the elementary probability of the cooperative energy transfer from Nd^{3+} (donor) to the cooperative pair acceptor (Ce_2) as $W_{\text{Nd} \rightarrow 2\text{Ce}}^0 =$

$W_{\text{Nd} \rightarrow 2\text{Ce}}^m(100\%)/6 = 262 \text{ s}^{-1}$, which is lower by a factor of several tens as compared to the value for the traditional energy transfer mechanism. According to theory of statistical energy transfer [2, 3], the latter estimate determines a boundary of the time interval $t_1 = (W^0)^{-1} = 3.8 \text{ ms}$ in which the luminescence decay kinetics has an exponential shape.

A nonlinear concentration quenching, similar to that described above, was observed upon excitation of the $^4I_{13/2}$ level of Er^{3+} ions in $\text{La}_{1-x}\text{Ce}_x\text{F}_3$ solid solution crystals, for which the traditional energy transfer is also forbidden and only the cooperative mechanism can be operative. Figure 4a (open circles) shows the dependence of the lifetime $\tau(^4I_{13/2})$ as function of the concentration of erbium ions. Figure 4b (black circles) presents the corresponding values of the rate of cooperative quenching $W_{\text{Er} \rightarrow 3\text{Ce}}(x) = 1/\tau(x) - 1/\tau(0)$. The solid curve in Fig. 4b shows approximation of the experimental data by the quenching rate plotted as a cubic function of the concentration of cerium ion, and the dashed line represents the linear quenching law. As seen from this figure, the cubic curve provides a sufficiently good fit to experiment, showing evidence of the cooperative nonradiative energy transfer from a single erbium ion simultaneously to three cerium ions representing a cooperative acceptor (Ce_3). The total rate of the cooperative energy transfer (CeF_3) was

$W_{\text{Nd} \rightarrow 3\text{Ce}}^m(100\%) = 120 \text{ s}^{-1}$, which is by one order of magnitude lower as compared to the analogous value for the cooperative quenching $\text{Nd} \rightarrow 2\text{Ce}$ in the case of cooperative pair acceptors and by two orders of magnitude as compared to the traditional linear mechanism of energy transfer $\text{Er} \rightarrow \text{Ce}$ or $\text{Nd} \rightarrow \text{Nd}$.

Similarly to the above analysis, by considering triads of Ce^{3+} ions as independent cooperative acceptors forming the nearest environment of an impurity donor ion (Er^{3+}) in CeF_3 lattice and assuming the number of nearest-neighbor acceptors equal to $12/3 = 4$, we may estimate the elementary probability of the nontraditional cooperative energy transfer from Er^{3+} (donor) to the cooperative triple acceptor (Ce_3) at a minimum distance as $W_{\text{Er} \rightarrow 3\text{Ce}}^0 = W_{\text{Er} \rightarrow 3\text{Ce}}^m(100\%)/4 = 30 \text{ s}^{-1}$.

CONCLUSION

We have experimentally observed a new phenomenon—nonlinear cooperative nonradiative energy transfer (cooperative concentration quenching or cooperative cross-relaxation) from a single excited neodymium ion simultaneously to a pair of cerium ions, representing a cooperative acceptor, and from a single erbium ion simultaneously to three cerium atoms also forming a cooperative acceptor center. The macroscopic rates of the cooperative energy transfer were determined for various concentrations of pair and triple cooperative acceptors. It is demonstrated that the total luminescence decay rate for the cooperative pair acceptor quenching $W_{\text{Nd} \rightarrow 2\text{Ce}}^m(100\%)$ in CeF_3 crystals is lower by a factor of several tens, and that for the cooperative triple acceptor quenching $W_{\text{Er} \rightarrow 3\text{Ce}}^m(100\%)$, by several hundreds, as compared to the total macroscopic rates of energy transfer $W_{\text{Er} \rightarrow \text{Ce}}^m(100\%)$ is or $W_{\text{Nd} \rightarrow \text{Ce}}^m(100\%)$ by the traditional mechanism of quenching transitions involving usual single acceptors. The elementary probability of the cooperative energy transfer was determined for the process involving two or three cerium ions forming cooperative quenchers at a minimum distance in the CeF_3 lattice.

REFERENCES

1. D. L. Dexter, *J. Chem. Phys.* **21**, 836 (1953).
2. V. P. Sakun, *Fiz. Tverd. Tela* **14** (8), 2199 (1972).
3. O. K. Alimov, M. Kh. Ashurov, T. T. Basiev, *et al.*, *Tr. Inst. Obshch. Fiz. Akad. Nauk SSSR* **9**, 50 (1987).
4. P. P. Feofilov and V. V. Ovsyankin, *Appl. Opt.* **6**, 1828 (1967).
5. L. D. Livanova, I. G. Saitkulov, and A. L. Stolov, *Fiz. Tverd. Tela* **11**, 918 (1969).
6. F. W. Ostermayer and L. G. Van Uitert, *Phys. Rev. B: Solid State* **1**, 4208 (1970).
7. T. T. Basiev and Yu. V. Orlovskii, *Zh. Éksp. Teor. Fiz.* **96**, 1965 (1989).
8. T. T. Basiev, Yu. V. Orlovskii, and Yu. S. Privis, *J. Lumin.* **69**, 187 (1966).

Translated by P. Pozdeev